


ORIGINAL ARTICLE

Muscleblind-like 2 knockout shifts adducin 1 isoform expression and alters dendritic spine dynamics of cortical neurons during brain development

Chia-Wei Huang¹ | Kuang-Yung Lee^{2,3} | Peng-Tzu Lin¹ | Fang-Shin Nian^{1,4} |
Haw-Yuan Cheng¹ | Chien-Hui Chang¹ | Cheng-Yen Liao^{1,5} | Yen-Lin Su¹ |
Carol Seah² | Ching Li² | Yu-Fu Chen² | Mei-Hsuan Lee⁴ | Jin-Wu Tsai^{1,6,7} 

¹Institute of Brain Science, College of Medicine, National Yang Ming Chiao Tung University, Taipei, Taiwan

²Department of Neurology, Chang Gung Memorial Hospital, Keelung Branch, Keelung, Taiwan

³Chang Gung University, College of Medicine, Taoyuan, Taiwan

⁴Institute of Clinical Medicine, College of Medicine, National Yang Ming Chiao Tung University, Taipei, Taiwan

⁵Faculty of Medicine, College of Medicine, National Yang Ming Chiao Tung University, Taipei, Taiwan

⁶Brain Research Center, National Yang Ming Chiao Tung University, Taipei, Taiwan

⁷Department of Biological Science and Technology, College of Biological Science and Technology, National Yang Ming Chiao Tung University, Hsinchu, Taiwan

Correspondence

Kuang-Yung Lee, Department of Neurology,
Chang Gung Memorial Hospital, Keelung
Branch, No. 222, Mai-Chin Rd., Keelung
20401, Taiwan.

Email: kylee@cgmh.org.tw;

kyleemdphd@gmail.com

Jin-Wu Tsai, Institute of Brain Science, College
of Medicine, National Yang Ming Chiao Tung
University, No.155, Sec.2, Linong Street,
Taipei 112, Taiwan.

Email: tsaijw@nycu.edu.tw

Funding information

National Health Research Institutes, Taiwan,
Grant/Award Number: NHRI-EX109-10904NI;
Ministry of Science and Technology, Taiwan,
Grant/Award Numbers: 110-2628-B-A49A-
506, 108-2321-B-010-011-MY2,
108-2638-B-010-001-MY2, 107-2221-E-
010-014; Taipei Veterans General Hospital-
University System of Taiwan, Grant/Award
Number: VGHUST110-G1-5-3; Brain Research
Center, National Yang Ming Chiao Tung
University (NYCU); ASUSTeK Computer Inc.,
Grant/Award Number: 110J041; Chang Gung
Memorial Hospital, Keelung Branch,
Grant/Award Number: CMRPG2F0502;
Ministry of Education, Taiwan

Abstract

Aims: Muscleblind-like 2 (MBNL2) plays a crucial role in regulating alternative splicing during development and mouse loss of MBNL2 recapitulates brain phenotypes in myotonic dystrophy (DM). However, the mechanisms underlying DM neuropathogenesis during brain development remain unclear. In this study, we aim to investigate the impact of MBNL2 elimination on neuronal development by *Mbnl2* conditional knockout (CKO) mouse models.

Methods: To create *Mbnl2* knockout neurons, cDNA encoding Cre-recombinase was delivered into neural progenitors of *Mbnl2*^{flax/flax} mouse brains by in utero electroporation. The morphologies and dynamics of dendritic spines were monitored by confocal and two-photon microscopy in brain slices and live animals from the neonatal period into adulthood. To investigate the underlying molecular mechanism, we further detected the changes in the splicing and molecular interactions of proteins associated with spinogenesis.

Results: We found that *Mbnl2* knockout in cortical neurons decreased dendritic spine density and dynamics in adolescent mice. *Mbnl2* ablation caused the adducin 1 (ADD1) isoform to switch from adult to fetal with a frameshift, and the truncated ADD1 failed to interact with alpha-II spectrin (SPTAN1), a critical protein for spinogenesis. In addition, expression of ADD1 adult isoform compensated for the reduced dendritic spine density in cortical neurons deprived of MBNL2.

Chia-Wei Huang and Kuang-Yung Lee contributed equally to this work.

This is an open access article under the terms of the [Creative Commons Attribution](https://creativecommons.org/licenses/by/4.0/) License, which permits use, distribution and reproduction in any medium, provided the original work is properly cited.

© 2023 The Authors. *Neuropathology and Applied Neurobiology* published by John Wiley & Sons Ltd on behalf of British Neuropathological Society.

Conclusion: MBNL2 plays a critical role in maintaining the dynamics and homeostasis of dendritic spines in the developing brain. Mis-splicing of downstream ADD1 may account for the alterations and contribute to the DM brain pathogenesis.

KEYWORDS

Add1, adducin, alternative splicing, dendritic spine, neural development, muscleblind-like, myotonic dystrophy

INTRODUCTION

Myotonic dystrophy (dystrophia myotonica, DM) is the most common muscular dystrophy in adults with a prevalence ranging from 0.5 to 180 in 100,000, with a relatively higher prevalence in Europeans and their descendants.^{1–3} DM is an autosomal dominant inherited disease with multi-systemic involvement, including skeletal muscle atrophy and myotonia, respiratory failure, heart conduction defects and dysfunction of the central nervous system (CNS).^{4,5} Two types of DM, type 1 (DM1) and type 2 (DM2), are caused by mutations on two different genes,^{6–10} either (CTG) trinucleotide repeats in the 3' untranslated region (3'-UTR) of *DMPK* (myotonic dystrophy protein kinase) gene in DM1 or (CCTG) tetranucleotide repeats in the first intron of *CNBP* (cellular nucleic acid-binding protein) in DM2.^{1,5,11}

The molecular pathogenesis of DM is through direct sequestration of RNA-binding protein Muscleblind-like (MBNL)¹² or indirect stabilisation of CUGBP Elav-like family member 1 (CELF1, also known as CUGBP) by the microsatellite repeat expansions.¹³ Particularly, the MBNL family of proteins colocalises with RNA foci, which accumulate in the nuclei, and subsequently, the function of MBNLs on RNA processing is affected.^{12,14,15} To test the hypotheses of MBNL loss of function in DM, *Mbnl* KO mouse models were generated and successfully reproduced myotonia, muscle pathology, cardiac conduction delay, respiratory distress, REM sleep misregulation and impaired spatial learning ability.^{16–19}

CNS manifestations severely compromise DM patients' capability of handling complex tasks and their quality of life^{2,5,20}; either in congenital, infantile and adolescent DM patients⁵ who show learning disability, autism spectrum disorders (ASD) and attention-deficit hyperactivity disorder (ADHD) or excessive daytime sleepiness, depression, apathy, dysexecutive syndrome, social avoidance, and fatigue in adult DM1 and DM2.^{5,21} Although advances in magnetic resonance (MR) brain imaging on DM patients and microstructural analysis in mouse models have been achieved in the past few years,^{22–26} there is still a huge gap between DM brain phenotypes and the misregulations of gene expression. In particular, it remains unclear how dysfunctions in MBNL-mediated splicing cause DM CNS phenotypes and affect neuronal microstructures.

In this study, we used in utero electroporation (IUE) of Cre-recombinase in *Mbnl2*^{flox/flox} (*Mbnl2*^{f/f}) mice to knock out *Mbnl2* in neural progenitors and their progeny cells and aimed to examine the dynamics of synapses by two-photon microscopy in live animals. We found evidence of dendritic spine abnormality, both in spine density and dynamics, during the course of brain development. We found the

Key Points

- Loss of MBNL2 in cortical neurons leads to a reduction of dendritic spine density and abnormal spine dynamics in adolescent mice.
- *Mbnl2* KO shifts ADD1 to fetal isoform, which reduced the ability to interact with SPTAN1.
- Expression of ADD1 adult isoform restores the dendritic spine density in *Mbnl2* KO neurons.
- ADD1 isoform shift may contribute to neuronal defects in the mouse model of myotonic dystrophy.

MBNL2 deficiency caused a splicing shift of *Add1* mRNA toward the fetal isoform, which in turn altered the phosphorylation and binding of *Add1* mRNA product adducin 1 (ADD1) to cytoskeletal protein alpha-II spectrin (SPTAN1). These morphological and molecular changes caused by MBNL2 elimination in the developing neurons may consequently contribute to DM brain pathogenesis.

MATERIAL AND METHODS

Animal model

The *Mbnl2*^{f/f} mouse model was originally generated and gifted by Dr. Maurice Swanson in the Department of Molecular Genetics and Microbiology, University of Florida (Gainesville, FL, USA).¹⁶ The wild-type (WT), heterozygous and homozygous floxed *Mbnl2* alleles were confirmed by genotyping and noted as *Mbnl2*^{+/+}, *Mbnl2*^{+/f} and *Mbnl2*^{f/f}, respectively. *Mbnl2* conditional knockout (*Mbnl2*^{f/f}; *Nestin-Cre*^{+/-} or *Nestin-Cre* CKO or CKO) models were generated by mating the *Nestin-Cre* line with conditional *Mbnl2*^{f/f}, as previously reported.^{26,27}

IUE

The detailed procedures of IUE have been published elsewhere.^{28–30} Briefly, mice were anaesthetised with isoflurane (induction: 4% supplied by chamber; maintenance: 1.5%–2% supplied by mask), and an incision was made through the skin and the abdominal muscle in

order to expose the underlying viscera. Each embryo was randomly injected with ~0.5 µL of plasmid DNA (final concentration for *Mbnl2* knockout: 1.5 µg/µL pCALNL-GFP + 0.5 µg/µL pCAG-Cre; or final concentration for *Add1* expression: 1.5 µg/µL pCALNL-GFP + 1.5 µg/µL pCALNL-Add1-IRES-GFP + 0.5 µg/µL pCAG-Cre) into the lateral ventricle on one side of the brain. Electroporation was then carried out at a voltage of 40 V, with five 50 ms pulses separated by 450 ms intervals. After electroporation, the uterine horns were placed back into the abdominal cavity carefully, and the incision was closed by sutures. The embryos were allowed to develop in the uterus, and pups were born through normal spontaneous delivery. The brains of the electroporated mice were harvested at E18.5, P1, P7, P14, P21, P30 and P90.

Constructs for knockout and overexpression

pCAG-Cre and pCALNL-GFP were gifts from Connie Cepko (Addgene, plasmid #13775 and #13770) and were used for *Mbnl2* IUE-mediated knockout. The pCAG-Cre expresses Cre recombinase only in the electroporated neural progenitors (i.e., radial glial cells). The pCALNL-GFP is composed of SV40 poly(A) stop signal floxed by two LoxP sites, upstream of the IRES-GFP sequence that allows the expression of GFP and labels the electroporated cells. *Add1* cDNA construct was designed, synthesised and then cloned into pCALNL-GFP by GenScript (New Jersey, USA). This gene was termed pCALNL-Add1-IRES-GFP.

Brain section and immunofluorescence staining

Immunofluorescence staining of brain slices was performed as previously described.^{31,32} Brains were perfused and immersed with 4% paraformaldehyde (PFA), embedded in agarose gel and sectioned by vibratome (Leica). Slices were washed with phosphate buffered saline (PBS), followed by phosphate buffered saline with Triton X-100 (PBST, 0.2% of Triton X-100 in PBS) permeabilization for 30 min. Next, brain slices were incubated in blocking buffer (5% bovine serum albumin [BSA] and 5% normal goat serum [NGS] in PBST) for 1 h and then incubated with primary antibodies dissolved in diluted blocking buffer (2.5% BSA and 2.5% NGS in PBST) at 4°C for 2 days. The sources of primary antibodies used in this study were listed as follows: anti-calretinin rabbit polyclonal antibody (1:250, Abcam, ab702), anti-calbindin rabbit polyclonal antibody (1:250, Abcam, ab11426), anti-NeuN rabbit polyclonal antibody (1:500, Millipore, ABN78), anti-BRN2 mouse monoclonal antibody (1:500; Santa Cruz Biotechnology, sc-393324), anti-OLIG2 rabbit polyclonal antibody (1:1000, Novus Biologicals, NBP1-28667), anti-GFAP rabbit polyclonal antibody (1:1000, Agilent Dako, Z0334), anti-IBA1 rabbit polyclonal antibody (1:1000, FUJIFILM Wako, 019-19741), anti-MBNL2 (3B4) mouse monoclonal antibody (1:1000, Santa Cruz, sc-136167) and anti-MBP rabbit monoclonal antibody (1:5000, Abcam, ab218011). Afterwards, sections were washed with PBS and incubated with fluorescent-dye conjugated secondary antibodies Alexa

Fluor™ 546 (1:500, Thermo Fisher Scientific, A-11010) for 2 h. Finally, samples were stained with DAPI (4',6-diamidino-2-phenylindole) at room temperature for 2 h and mounted with VECTASHIELD® Mounting Media (Vector Laboratories, H-1000).

Protein lysis and western blot analysis

The cortex tissue was lysed in RIPA buffer (Sigma-Aldrich, R0278) containing 10% protease inhibitor (Sigma-Aldrich, 04693159001) and 10% phosphatase (Sigma-Aldrich, 04906837001). The protein concentration was quantified by Pierce™ BCA Protein Assay Kit (Thermo Fisher Scientific, 23225). Protein samples (80 µg/lane) were separated by 8% or 4%–20% gradient SDS polyacrylamide gel electrophoresis (SDS-PAGE) (BIOTOOLS, TFU-GG420) under constant voltage of 100 V and then transferred onto the polyvinylidene fluoride (PVDF) membrane (Millipore) with transfer buffer containing 10% or 15% methanol under constant voltage of 100 V for 2 h. The membranes were incubated in the blocking buffer (5% skim milk in tris buffered saline with tween 20 [TBST, 0.1% Tween-20 in tris buffered saline]) at room temperature for 1 h and then incubated in the primary antibody dissolved in the blocking buffer at 4°C overnight. The primary antibodies were as follows: anti-ADD1 rabbit polyclonal antibody (1:1000, GeneTex, GTX101600), anti-TANC2 rabbit polyclonal antibody (1:1000, Novus Biologicals, NBP1-85087), anti-MBNL2 (3B4) mouse monoclonal antibody (1:1000, Santa Cruz, sc-136,167), anti-alpha tubulin mouse monoclonal antibody (1:5000, Proteintech, 66,031-1-Ig) and anti-PSD93 rabbit monoclonal antibody [EPR8740] (1:1000, Abcam, ab151721). The immunoblots were washed with TBST buffer and incubated at room temperature for 2 h in blocking buffer containing goat anti-mouse IgG-HRP (1:10000, Millipore, AP124P) or goat anti-rabbit IgG-HRP (1:10000, Sigma-Aldrich, A0545). The signals on the membrane were generated by Immobilon Western Chemiluminescent HRP Substrate (Millipore, WBMLS0500) and detected by luminescence imaging system LAS-4000 (Fujifilm). At last, the results were quantified by ImageJ software (National Institutes of Health [NIH], USA) and analysed by GraphPad Prism 8 software.

Dendritic spine imaging and analysis

Mouse brains electroporated with pCALNL-GFP and pCAG-Cre constructs were fixed and sectioned. Six to eight brain slices of each mouse were then mounted. Next, 10 to 15 basal dendrites of cortical layer II/III neurons from the somatosensory cortex were randomly selected and imaged with confocal microscopy (LSM700/LSM880, Carl Zeiss), and the dendrites were analysed using semi-automated³³ and artificial intelligence (AI)-assisted algorithms (NYCU-ASUSTeK). Spine density results were acquired through the analysis of thousands of dendritic spines from more than three mice in each group. Since the structure of dendritic spines was small, the frame size of each image was unified as 1024 (X)*1024 (Y), and the size of each pixel was controlled as 0.078 µm*0.078 µm*0.42 µm (X, Y, Z).

Thinned-skull cranial window and in vivo two-photon imaging

The procedure of thinned-skull preparation was described previously.³⁴ Briefly, a round region of the skull 1 mm in diameter above the somatosensory cortex was thinned into 20–30 μm in each mouse without causing microbleeds or skull damage. All mice underwent surgeries twice on experimental day 0 and day 2. Apical dendrites extending from GFP⁺ pyramidal neurons (about 20 apical dendrites from more than three mice in each group) were randomly selected and monitored by two-photon microscopy (7MP, Carl Zeiss). All images were scanned with frame size 512(X)*512(Y) and then analysed by using a semi-automated algorithm as described above. The size of each pixel was 0.208 μm *0.208 μm *0.638 μm (X, Y, Z). Neurons were positioned based on the nearby blood vessels under visible light. Mice with bleeding or trauma during surgery were abandoned owing to potential neuro-inflammation. To study the spine dynamics, statuses of dendritic spines were defined and calculated as follows: Formation rate (%) = the number of new spines/pre-existing spines; Elimination rate (%) = the number of eliminated spines/pre-existing spines; Stable rate (%) = the number of stable spines/pre-existing spines.

GST pull-down assay

Add1^{−ex15} and *Add1*^{+ex15} cDNA expressing constructs were originally designed and synthesised by BIOTOOLS (New Taipei City, Taiwan) and GenScript (New Jersey, USA). Both neck and tail domains of *Add1*^{−ex15} (NM_013457.4, 350–735 a.a.) or *Add1*^{+ex15} (NM_001024458.4, 350–747 a.a. with a pre-mature STOP codon and 350–632 a.a.) cDNA were cloned into the pGEX4T-1 construct. The method for generating GST-tagged protein using *Escherichia coli* has been previously described (Tsai et al, 2020). The E18.5 WT mouse brain lysates were incubated with glutathione resins conjugated with neck and tail domains of *ADD1*^{−ex15} or *ADD1*^{+ex15} overnight at 4°C. Western blotting was used to identify the interaction between *ADD1* and SPTAN1 with an anti- α -II spectrin antibody (Santa Cruz, sc-48382).

In situ hybridization

A digoxigenin-labelled antisense RNA probe for *Mbnl2* mRNA was prepared according to the manufacturer's instructions (Roche). The sequence of the *Mbnl2* probe was obtained from the Allen Institute for Brain Science (<https://portal.brain-map.org/>). Brain samples for in situ hybridization were derived from 2 months old *Mbnl2*^{+/+} and *Mbnl2*^{f/f} mice electroporated with mixed plasmids (pCALNL-GFP + pCAG-Cre constructs). These samples were fixed by 4% PFA in PBS (pH 7.4) at 4°C overnight. The brains were then placed in 30% sucrose for 1 day until brains sank into the bottom of the tube and cryo-sectioned into coronal sections of 14 μm in thickness. The sections were then hybridised with 1 $\mu\text{g}/\text{mL}$ of DIG-labelled antisense RNA probe at 60°C overnight. The hybridization signals were detected by

alkaline phosphatase (AP) conjugated anti-digoxigenin-AP, Fab fragments (1:250, Roche, 11093274910) and then visualised with NBT/BCIP reagent (Roche, 11697471001). The GFP signal was amplified by the anti-GFP antibody (1:500, Abcam, ab13970). Images were analysed using ImageJ (NIH, USA).

Detection of phosphorylated Add1 protein

pEGFP-*Add1*^{−ex15} or pEGFP-*Add1*^{+ex15} were transfected into HEK293T cells and cell lysates were collected 24 h after transfection. EGFP-fused *ADD1*^{−ex15}/*ADD1*^{+ex15} proteins were pulled down by GFP-Trap magnetic beads (ChromoTek, gtma-100) and analysed by western blotting. Phosphorylated and total *Add1* proteins were detected by anti-phospho-(Ser/Thr) Phe antibody (1:1000, Abcam, ab17464) and anti-GFP antibody (1:5000, Proteintech, 50430-2-AP), respectively. The quantification was performed by using ImageJ (NIH, USA).

RT-PCR analysis for isoform changes

Fresh brains electroporated with pCALNL-GFP and pCAG-Cre by in utero electroporation were collected from P30 *Mbnl2*^{f/f} mice. These brains were immediately transferred into the RNeasy Lysis Solution (Qiagen) and immersed for 2 h. Tissue samples from electroporated and contralateral sides, consisting of GFP⁺ *Mbnl2* KO (30%–50% purity) and WT cells, respectively, were dissected from layer II/III cortex. Total RNAs were extracted by TOOLSsmart RNA Extractor (BIOTOOLS, DPT-BD24) and reverse-transcribed (25 ng RNA/sample) with a mix of Oligo (dT) and random primers (Solis BioDyne, 06-20-00500). Isoforms of gene targets were amplified from cDNA by PCR. Specific primers for targets were as previously described.¹⁶ Amplified cDNAs were further analysed by DNA electrophoresis and ImageJ (NIH, USA).

Statistical analysis

All data were statistically analysed with GraphPad Prism (version 8.0) and Excel (Microsoft). All details and further information regarding the types of tests utilised, the number of biological replicates performed, the number of animals used, and the number and sampling of images analysed are described in figure legends.

RESULTS

Macro-structures of the hippocampus and cerebral cortex in *Mbnl2* KO mice

Since spatial learning deficits were observed in *Mbnl2* ^{$\Delta\text{E2}/\Delta\text{E2}$} mice,¹⁶ we first examined the development of hippocampal neurons, which

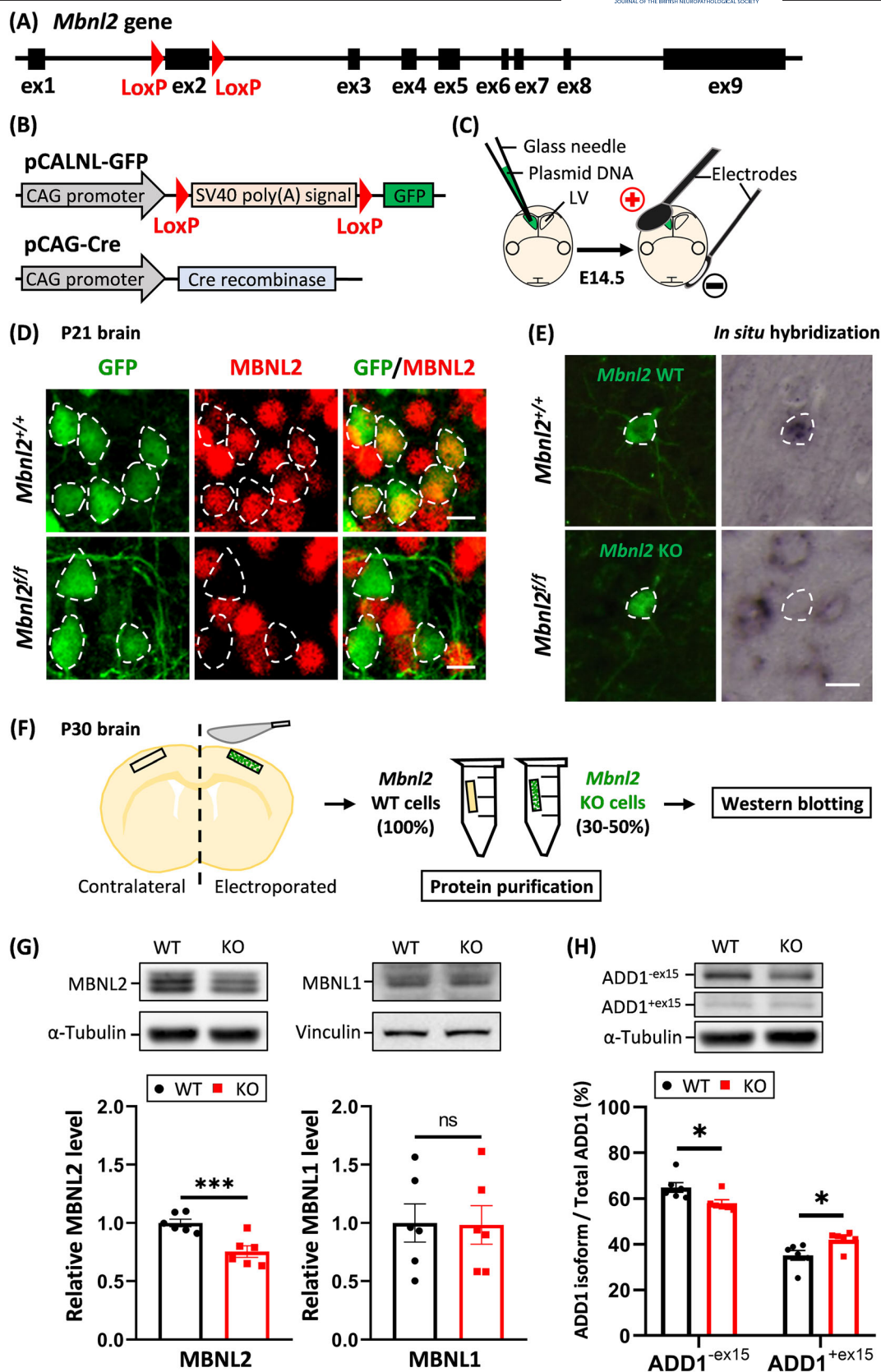


FIGURE 1 Legend on next page.

FIGURE 1 Expression of MBNL2, MBNL1, ADD1^{-ex15} and ADD1^{+ex15} in electroporated *Mbnl2*^{+/f} cortical tissue. (A) Schematic diagram of floxed allele in *Mbnl2*^{+/f} mice. Exon 2 (ex2, black box) of *Mbnl2* was flanked by two LoxP sites (red triangle). (B) Schematic diagram of pCALNL-GFP (top) and pCAG-Cre (bottom) constructs. The SV40 poly(A) stop signal was flanked by two LoxP sites and located upstream of the GFP-coding region in pCALNL-GFP. (C) Procedure for IUE. Plasmid DNA was injected into the lateral ventricle (LV) of the developing cortex with fast green dye and electroporated into neural progenitors in mice at E14.5. Red (+): Positive electrode; black (-): Negative electrode. (D) Immunofluorescence staining of MBNL2 (red) in the brain sections from *Mbnl2*^{+/+} and *Mbnl2*^{+/f} mice at P21. MBNL2 expression is much lower in GFP⁺ cortical neurons (green, dotted circle) electroporated with pCALNL-GFP and pCAG-Cre in *Mbnl2*^{+/f} mice (bottom). Bar = 10 μ m. (E) In situ hybridization of *Mbnl2* in brain slices at 2 months old. *Mbnl2* mRNA was decreased in GFP⁺ cortical neurons (green, dotted circle) electroporated with Cre in *Mbnl2*^{+/f} mouse. Bar = 15 μ m. (F) Procedure of tissue preparation and protein analysis of MBNL2 in electroporated *Mbnl2*^{+/f} brain tissue. Brain tissue of the cortex containing GFP⁺ cells (KO, 30%–50% purity) and the contralateral side (WT, 100% purity) were dissected and lysed for western blotting. (G) Expression of MBNL1 and MBNL2 in electroporated cortical tissue from *Mbnl2*^{+/f} mice at P30. The bar and dots graph shows a significant decrease in relative MBNL2 expression in electroporated cortical tissue. There was no significant difference in MBNL1 expression. (H) Expression of fetal and adult ADD1 isoforms in electroporated cortical tissue versus the contralateral side at P30. The bar and dots graph shows the expression of ADD1 fetal isoform was significantly higher in Cre-electroporated cortical tissue compared to the contralateral side. ($n = 6$ in each group). Error bars represent SEM. Paired Student's t-test. * $p < 0.05$, *** $p < 0.001$. Abbreviation: ns, not significant.

have been implicated in the formation of spatial memory.³⁵ Brains from *Mbnl2* CKO mice were stained with calbindin 2 (a.k.a. calretinin, a marker for immature granule neurons) and calbindin (a marker for mature neurons) antibodies at postnatal days (P) 23 and 34, respectively^{36,37} (Figure S1). We found that at P23, calbindin 2 was readily detectable in the inner molecular layer (IML) and subgranular zone (SGZ) of the dentate gyrus (DG), in both *Mbnl2*^{+/f} and *Mbnl2*^{+/f}; *Nestin-Cre*^{+/-} mice (Figure S1A). At P34, pyramidal cells in CA1 and granule cells in CA3 and DG expressed comparable calbindin in both groups^{38,39} (Figure S1B). We also examined the general morphologies of the cerebral cortex in *Mbnl2*^{+/f} and *Mbnl2*^{+/f}; *Nestin-Cre*^{+/-} mice, including the thickness and area in brain sections (Figure S1C). We found no significant differences between these mice (Figure S1D), consistent with our previous study.²⁶ Therefore, from a macrostructural perspective, the early development from immature to mature neurons was not affected in the mouse hippocampal neurons that were devoid of MBNL2 in neural progenitor cells.

Because cognitive deficits in DM patients may also be related to cortical function, we then investigated the effects of MBNL2 loss of function on cortical development. We applied IUE to introduce cDNA expressing Cre-recombinase (pCAG-Cre) into neural progenitors (i.e., radial glial cells) in the developing cortex of *Mbnl2*^{+/+}, *Mbnl2*^{+/f} and *Mbnl2*^{+/f} mice at embryonic day 14.5 (E14.5) (Figure 1A–C), at which time radial glial cells produce mostly layer II/III pyramidal neurons. To track *Mbnl2* KO cells, we co-electroporated the brains with a Cre-dependent green fluorescent protein (GFP) construct pCALNL-GFP, in which an SV40 poly(A) terminator sequence flanked by two LoxP sites was inserted between the CAG promoter and GFP⁴⁰ (Figure 1B). Immunofluorescence staining and in situ hybridization of sections from electroporated brains showed the absence of *Mbnl2* protein and mRNA, respectively, in GFP⁺ cells in *Mbnl2*^{+/f} mice (Figure 1D, E). Western blotting of the lysate from electroporated brains (Figure 1F) also showed that protein expression of MBNL2, but not MBNL1, was lower in the electroporated brain tissue (Figure 1G), further supporting the knockout of *Mbnl2*. At P1, most electroporated GFP⁺ cells in *Mbnl2*^{+/+}, *Mbnl2*^{+/f}, and *Mbnl2*^{+/f} mice have migrated into cortical layer II/III (Figure 2A, B). To examine the neuronal lineage

of these GFP⁺ cells, electroporated brains were stained with BRN2 and NeuN, markers for cortical layer II, III (V)⁴¹ and neurons⁴² at P7 (Figure 2C, D). We found that most GFP⁺ neurons in *Mbnl2*^{+/f} mice still expressed BRN2 and NeuN, similar to those in *Mbnl2*^{+/+} mice.

Decreased spine density in adolescent *Mbnl2* KO neurons

Since there were no major changes in the main structures of the hippocampus and cortical neurons, we then examined whether neuronal connectivity is affected after *Mbnl2* ablation. Dendritic spines are critical postsynaptic structures that have been associated with multiple brain functions, such as learning and memory, motor and sensory functions, and social behaviours.⁴³ Therefore, we performed in utero electroporation and investigated the morphologies of *Mbnl2* KO neurons postnatally during childhood (P14), adolescence (P21 and 30) and adulthood (P90) (Figure 3A). Electroporated GFP⁺ cells showed typical morphology of pyramidal neurons with multiple dendritic branches extending toward superficial layers (Figure 3B). The complexity of dendritic branches was analysed by Sholl analysis at 1 and 3 months. We found the numbers of dendritic branches did not show significant differences among all groups (Figure S2A, B). Transcallosal axon projections towards the contralateral brain could also be readily observed (Figure S2C). The general structure of axons also did not show an apparent difference in all groups although ultrastructural changes may exist but could not be detected due to the limitation of optical resolution (Figure S2D).

The densities of dendritic spines that originated from these dendrites were analysed at P14, P21, P30 and P90 among *Mbnl2*^{+/+}, *Mbnl2*^{+/f} and *Mbnl2*^{+/f} groups (Figure 3C, D). At P14 (childhood) when the dendritic spines start to increase dramatically, there was no significant difference. Interestingly, at P21 and P30 (adolescence), the spine density of in *Mbnl2*^{+/f} mice were significantly decreased (P21: *Mbnl2*^{+/+}: $1.527 \pm 0.051 \mu\text{m}^{-1}$, $n = 3$; *Mbnl2*^{+/f}: $1.410 \pm 0.031 \mu\text{m}^{-1}$, $n = 3$; *Mbnl2*^{+/f}: $1.320 \pm 0.046 \mu\text{m}^{-1}$, $n = 5$; P30: *Mbnl2*^{+/+}: $1.053 \pm 0.040 \mu\text{m}^{-1}$, $n = 7$; *Mbnl2*^{+/f}: $0.990 \pm 0.017 \mu\text{m}^{-1}$, $n = 2$; *Mbnl2*^{+/f}: $0.862 \pm 0.052 \mu\text{m}^{-1}$, $n = 5$).

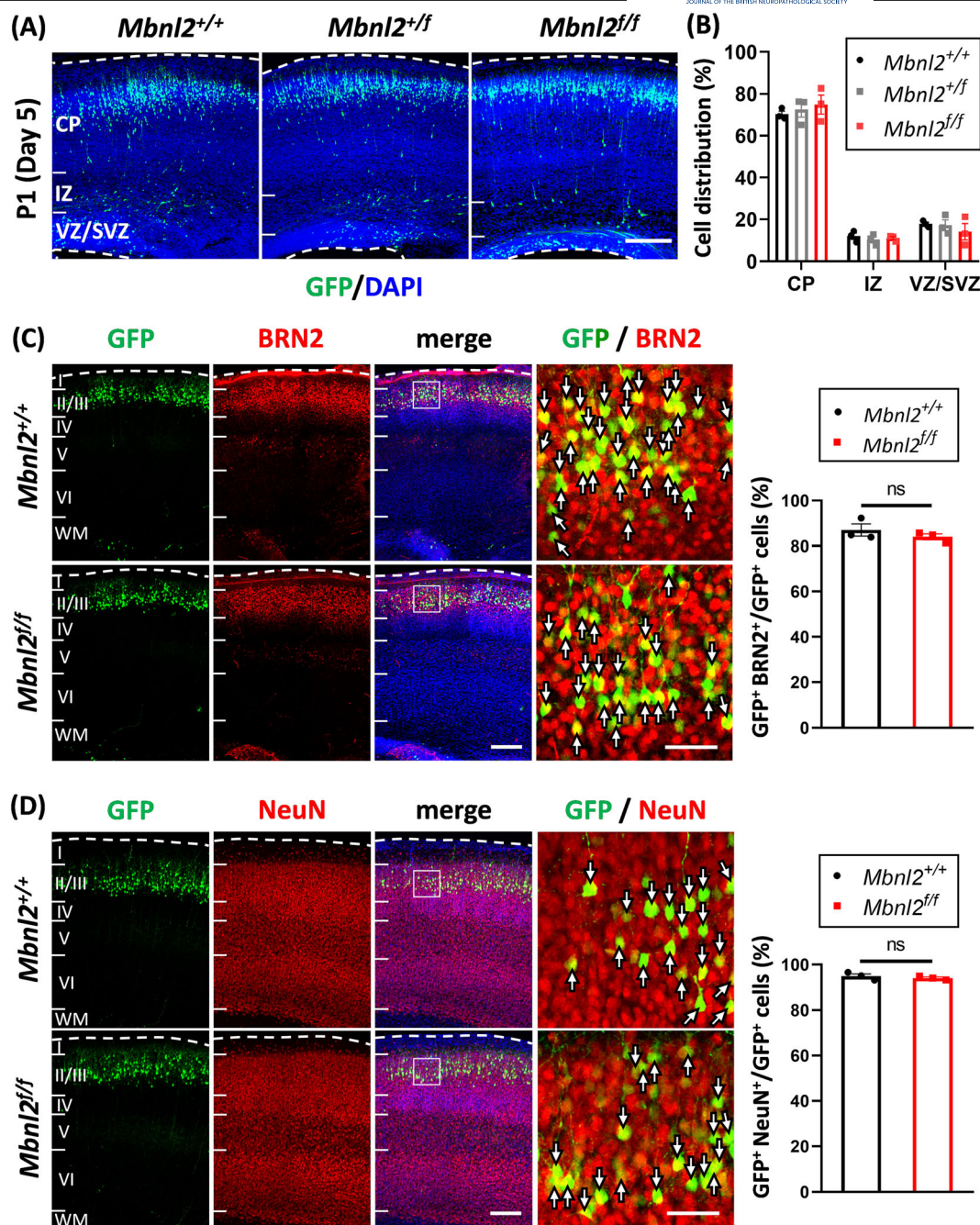


FIGURE 2 Migration and differentiation of *Mbnl2* KO neurons during cortical development. (A) Distributions of electroporated cells in the cerebral cortex of *Mbnl2*^{+/+}, *Mbnl2*^{+/f} and *Mbnl2*^{f/f} mice at P1. Coronal sections of the mouse brains were collected 5 days after IUE. Most of the GFP⁺ cells (green) in all genotypes have already reached the cortical plate (CP). Bar = 200 μ m. (B) Bar graph showing the percentage of GFP⁺ cells in the CP, IZ and VZ/SVZ regions of neocortex 5 days after electroporation ($n = 3$ mice). Error bars represent SEM. One-way ANOVA test. There is no significant difference between each genotype. (C) Immunofluorescence staining of BRN2 for layer II/III neurons (red) in electroporated cells (green) at P7. The majority of GFP⁺ cells were located in cortical layer II/III expressing BRN2 in both genotypes. Bar = 200 μ m. Right panel: High-magnification images from the boxes highlighting BRN2 expression in GFP⁺ cells (arrows) in the cortex. Bar = 50 μ m. Error bars represent SEM. Student's t-test with Welch's correction. (D) Expression of the late neuronal marker NeuN (red) in GFP⁺ cells (green) at P7. Most of the electroporated cells differentiated into neurons in both genotypes. Bar = 200 μ m. Right panel: High-magnification images from the boxes highlighting NeuN expression in GFP⁺ cells (arrows) in the cortex. Bar = 50 μ m. Error bars represent SEM. Student's t-test with Welch's correction. Abbreviation: ns, not significant.

Unexpectedly, the spine density of *Mbnl2* KO neurons had no significant difference compared to WT neurons at P90 (*Mbnl2*^{+/+}: $1.033 \pm 0.054 \mu\text{m}^{-1}$, $n = 4$; *Mbnl2*^{+/f}: $1.130 \pm 0.027 \mu\text{m}^{-1}$, $n = 3$; *Mbnl2*^{f/f}:

$1.066 \pm 0.047 \mu\text{m}^{-1}$, $n = 5$). These results suggested that *Mbnl2* knockout may lead to abnormal synaptic connection, particularly in adolescent mouse brains during brain development.

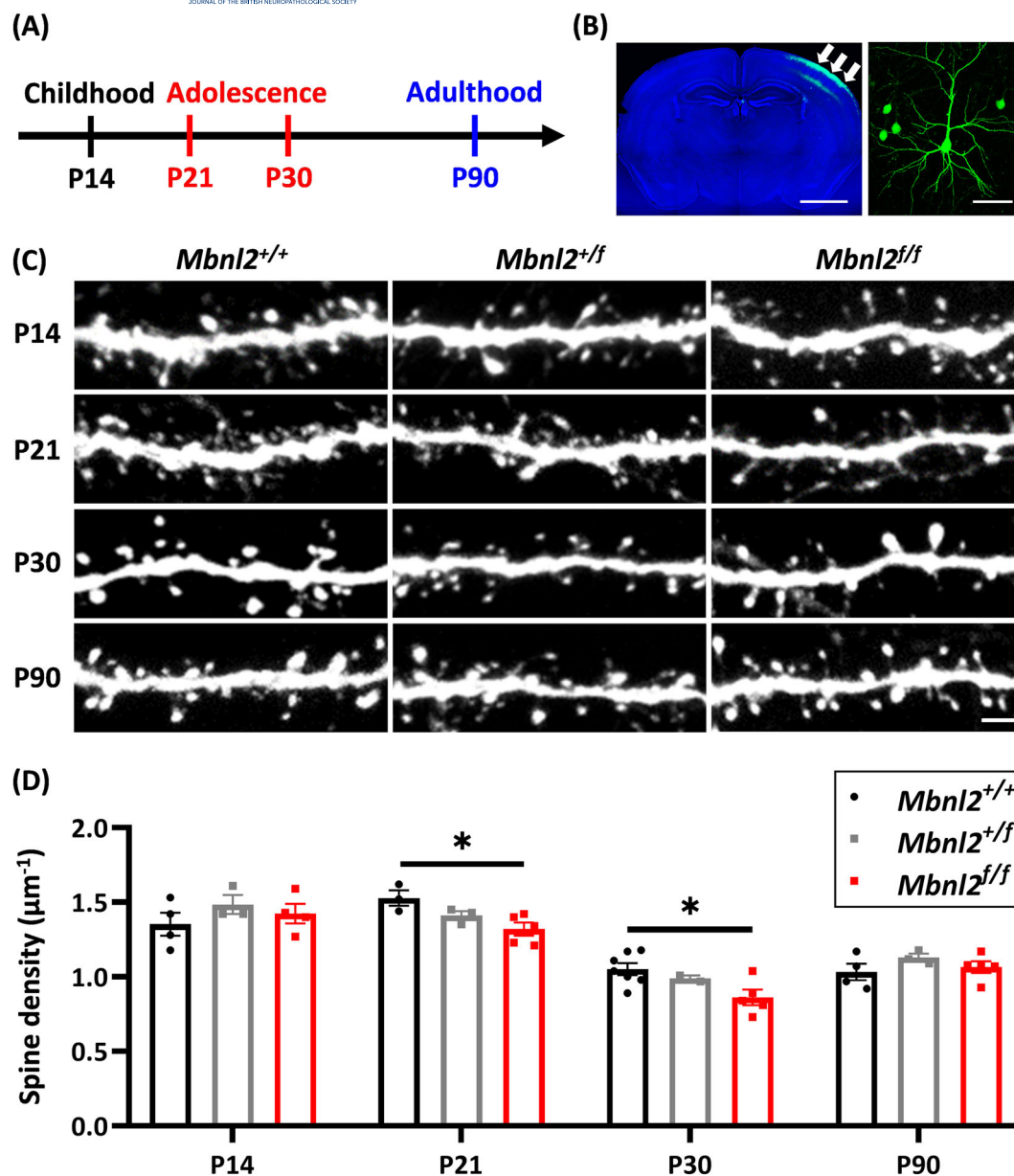


FIGURE 3 Decreased dendritic spine density in *Mbnl2* KO cortical neurons during early postnatal development. (A) Dendritic spines of GFP⁺ neurons in the cortex were imaged in childhood (P14), adolescence (P21 and P30) and adulthood (P90) in mice electroporated in utero with pCAG-Cre and pCALNL-GFP at E14.5. (B) A layer of electroporated GFP⁺ cortical neurons (green, white arrows) in the brain section stained with DAPI (blue). Bar = 2 mm (left panel). High-magnification image showing the morphology of an electroporated cortical neuron (green) with dendritic branches. Bar = 50 μm (right panel). (C) Images of typical dendrites with spines at P14, P21, P30 and P90 in *Mbnl2*^{+/+}, *Mbnl2*^{+/f} and *Mbnl2*^{f/f} mouse cortices. Significantly reductions in the dendritic spine densities were observed in *Mbnl2* KO cortical neurons at both P21 and P30. Bar = 2 μm (D) statistical analysis of dendritic spine density at P14, P21, P30 and P90. Error bars represent SEM. One-way ANOVA test. **p* < 0.05.

We further investigated whether *Mbnl2* knockout also affects different spine types, which are typically classified into filopodia, thin, stubby, and mushroom, based on morphology⁴⁴ (Figure S3A). We found that there was no significant difference in the composition of spines, either immature (e.g., filopodia) or mature (e.g., mushroom) type of spines, between *Mbnl2*^{+/+} and *Mbnl2*^{f/f} neurons at four different time points throughout the period from P14 and P90 (Figure S3B).

Since MBNL2 depletion in cell types other than neurons may interfere with the observed neuronal phenotypes, we tested whether depriving MBNL2 through IUE in *Mbnl2*^{f/f} mice may affect glial cell density and morphologies using immunofluorescence staining. Astrocytes were stained with GFAP (glial fibrillary acidic protein) in electroporated cortices at P21. We found that the morphology and density of astrocytes in electroporated *Mbnl2*^{f/f} cortices did not show differences compared to those in *Mbnl2*^{+/+} cortices (Figure S4A, B).

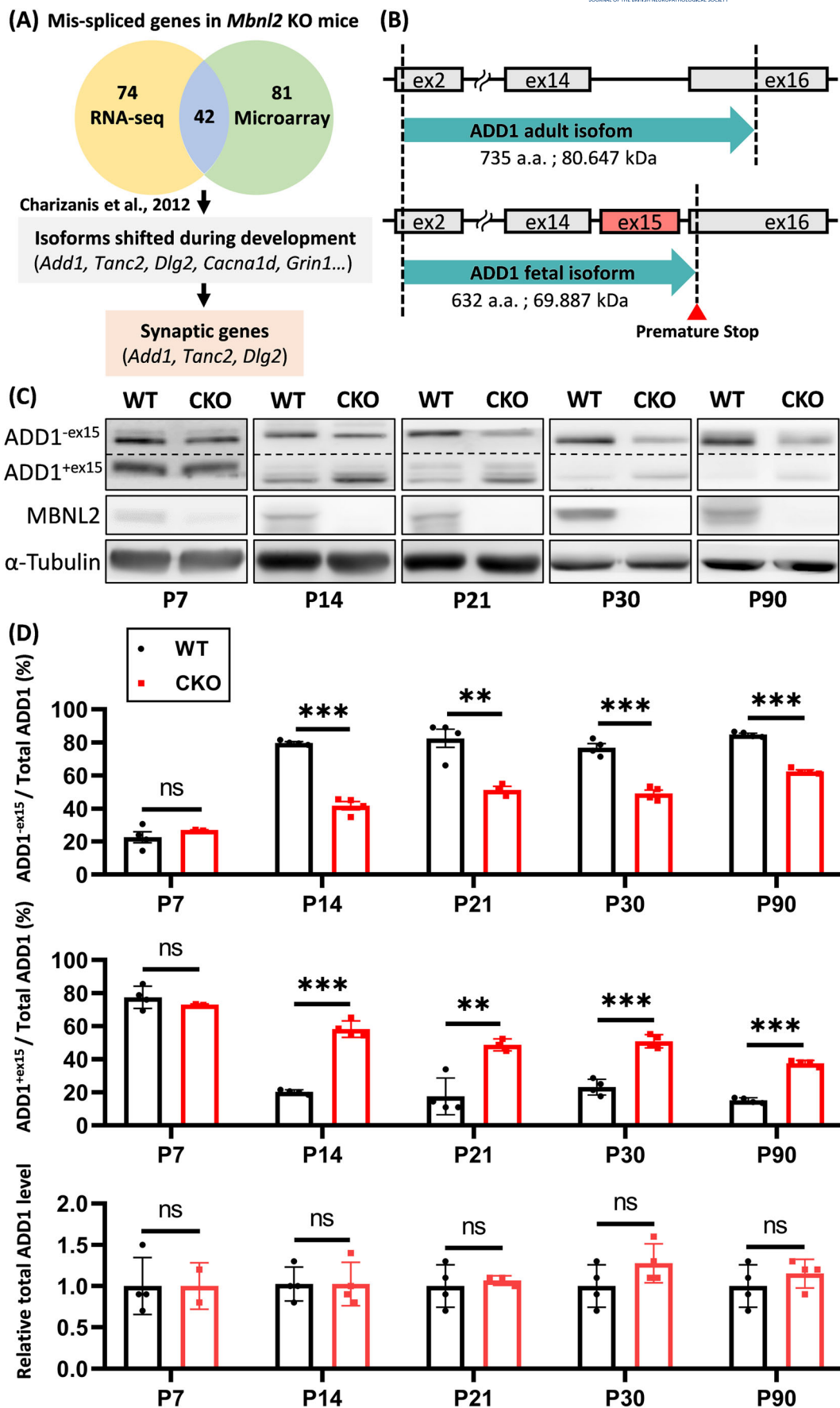


FIGURE 4 Legend on next page.

FIGURE 4 *Mbnl2* knockout affected ADD1 isoform expression in the developing cortex. (A) Flow chart of screening for potential target genes associated with *Mbnl2* knockout effects on dendritic spines. *Add1*, *Tanc2* and *Dlg2* are genes encoding synaptic proteins and are mis-spliced during brain development in *Mbnl2*^{ΔE2/ΔE2} mice. (B) Schematic diagram of ADD1 adult (ADD1^{−ex15}) and fetal (ADD1^{+ex15}) isoforms. Exon 15 (ex15) is spliced out in the adult ADD1 isoform. In the fetal isoform, the spliced-in of exon 15 leads to a premature stop and a truncated protein. (C) Expression of adducin 1 protein levels in the cerebral cortex of WT and *Mbnl2* CKO mice at different developmental time points. At P7, WT cortices express both adult and fetal isoforms. From P14 to P90, ADD1 expression gradually shifted to the adult isoform. However, in *Mbnl2* CKO cortices, the expression of fetal isoform remained, particularly high during adolescence. (D) Bar graphs showing relative expression of adducin 1 adult isoform, fetal isoform and the total protein expression. *n* ≥ 3 mice in both groups. Error bars represent SEM. Student's t-test with Welch's correction. **p* < 0.05, ***p* < 0.01, ****p* < 0.001. Abbreviation: ns, not significant.

Similarly, oligodendrocytes were stained with OLIG2 (oligodendrocyte transcription factor 2, oligodendrocyte lineage marker) and MBP (myelin basic protein, mature oligodendrocyte marker) for their nuclei and morphology. We did not find differences in the density and morphology of oligodendrocytes between electroporated *Mbnl2*^{+/+} and *Mbnl2*^{f/f} cortices (Figure S4C–E). Finally, microglia around electroporated cortical neurons were stained with IBA1 and showed no difference in the cell density and morphologies between electroporated *Mbnl2*^{+/+} and *Mbnl2*^{f/f} cortices (Figure S5).

Alternative splicing changes of *Add1* in *Mbnl2* KO mice

Previous studies revealed that constitutive loss of MBNL2 causes thousands of splicing changes in its downstream targets by RNA-seq and microarray. Forty-two highly ranked mis-spliced genes were found in both data sets. We found most affected genes switched the splicing pattern back to the fetal isoform in the adult mouse hippocampus.¹⁶ Among them, *Add1* (adducin 1), *Tanc2* (tetratricopeptide repeat, ankyrin repeat and coiled-coil containing 2) and *Dlg2* (discs large MAGUK scaffold protein 2, also known as PSD-93) were involved in dendritic spine development^{45–48} (Figure 4A). Thus, we first examined adult and fetal mRNA isoforms of *Add1*, *Tanc2* and *Dlg2* in Cre-electroporated brain tissue in *Mbnl2*^{f/f} mice at P30 using RT-PCR and validated a shift from adult to fetal isoform in all 3 genes (Figure S6).

It was previously demonstrated that MBNL2 inactivation leads to an *Add1* isoform shift with the inclusion of exon 15 (37 nucleotides),¹⁶ which causes a frameshift and introduction of a premature stop codon in exon 16 (Figure 4B). This change may potentially produce a truncated adducin 1 (ADD1) protein isoform of 632 a.a. (ADD1^{+ex15} at ~70 kDa) instead of the normal size of 735 a.a. (at ~81 kDa). Therefore, we examined the expression of these two isoforms in *Mbnl2* CKO mice at P7, P14, P21, P30 and P90 by western blotting (Figure 4C). In WT mice, significantly higher levels of the fetal ADD1^{+ex15} isoform were expressed in the cortex at P7 (before the robust expression of MBNL2). The relative level of the adult ADD1^{−ex15} isoform increased dramatically from P7 to P14. Remarkably, in the cortex of *Mbnl2* CKO mice, the protein expression level of ADD1^{+ex15} fetal isoform was significantly higher compared to the WT mice between P14 and P90, while total ADD1 expression remained

unchanged (Figure 4D). This result suggested that loss of MBNL2 indeed leads to changes in two different ADD1 protein isoforms. This isoform shift was further confirmed in *Mbnl2*^{f/f} brains electroporated with Cre recombinase (Figure 1H). We also examined expression changes of TANC2 and DLG2. However, their corresponding splicing shifts and exon inclusions caused by *Mbnl2* elimination did not cause frameshift or premature stop codon but added 10 and 14 amino acids to the proteins, respectively. These changes may only have a limited impact on protein expression, demonstrated in the western blotting (Figures S7 and S8).

Increased spinogenesis by ADD1 expression in *Mbnl2* KO neurons

Based on these results, we hypothesized that the isoform switch of ADD1 may contribute to the changes during dendritic spine development in *Mbnl2* KO neurons. Initially, a Cre-dependent ADD1 adult isoform-expressing construct (pCALNL-Add1-IRES-GFP) was first designed and tested in HEK293T cells (Figure 5A, B). We then co-electroporated pCALNL-Add1-IRES-GFP along with Cre-recombinase (pCAG-Cre) into *Mbnl2*^{f/f} mice and evaluated whether the expression of ADD1 adult isoform could rescue the decreased dendritic spine density. As expected, we found a significant increase in the spine density at P30 (Figure 5C, D), suggesting that overexpression of adult type ADD1 alone may potentially be helpful in correcting *Mbnl2* KO phenotypes on dendritic spine density.

Adducin 1 belongs to the adducin cytoskeletal protein family and forms a heterodimer with adducin 2 (ADD2, encoded by *Add2*). Previously, ADD2 was known to play an important role in synapse formation and dendritic spine maturation by interacting with spectrin through its C-terminal tail domain.^{48–50} To examine the impact of exon 15 inclusion on adducin 1 and its binding capability with spectrin, we generated cDNAs that express the C-terminus of adducin 1 adult and fetal isoforms with a GST tag (Figure 6A). GST pull-down assay was performed by using E18.5 WT mouse brain lysates in vitro. We found that the adducin 1 adult isoform possesses a stronger binding affinity with alpha-II spectrin (SPTAN1), compared to the fetal isoform, in which the C-terminal 103 amino acids are missing (Figure 6B, C). Interestingly, the C-terminus of the adducin 1 adult isoform contains several major phosphorylation sites; therefore, we examined whether overall protein phosphorylation was also changed in fetal

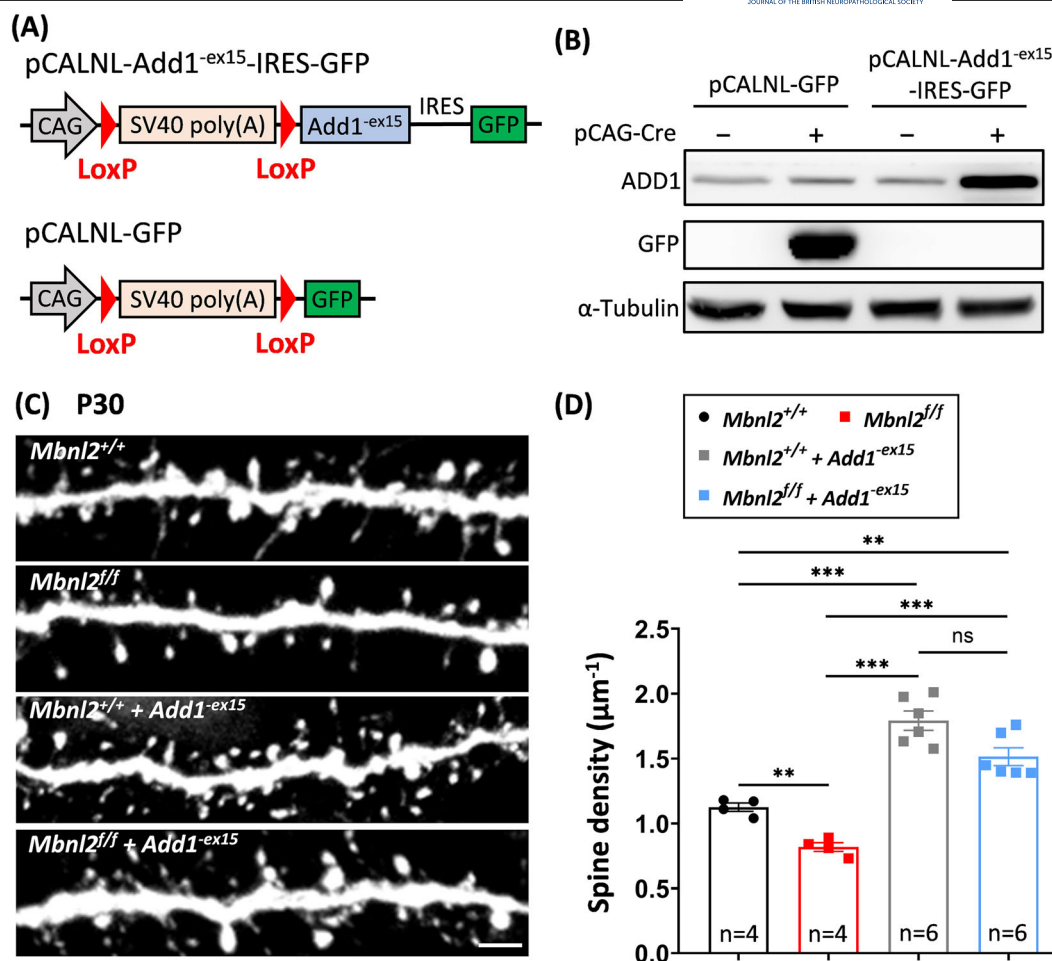


FIGURE 5 Adult-type ADD1 isoform overexpression increased dendritic spine density in *Mbnl2* KO cortical neurons. (A) Schematic diagram of pCALNL-GFP and pCALNL-Add1^{-ex15}-IRES-GFP constructs. Add1^{-ex15} cDNA was inserted into the site between the stop signal (SV40 poly(a) signal) and GFP. (B) pCALNL-Add1^{-ex15}-IRES-GFP or pCALNL-GFP with or without pCAG-Cre were transfected into HEK293T cells. The expression levels of adducin 1 and GFP were detected by western blotting. Overexpression of ADD1 or GFP was shown in cells co-transfected with pCAG-Cre. pCALNL-Add1^{-ex15}-IRES-GFP showed an unexpectedly low GFP expression, possibly due to low translation efficiency after the IRES. (C) Dendritic spines were imaged at P30 in brains co-electroporated with pCAG-Cre, pCALNL-GFP and pCALNL-Add1^{-ex15}-IRES-GFP in utero at E14.5. Increased dendritic spine densities were observed on dendrites in both WT and *Mbnl2* KO cortical neurons expressing ADD1^{-ex15} at P30. Scale bar = 2 μ m. (D) Bar and dot graphs of dendritic spine density with or without ADD1^{-ex15} expression at P30. One-way ANOVA test. **p* < 0.05, ***p* < 0.01, ****p* < 0.001. Abbreviation: ns, not significant.

adducin 1 in vitro (Figure 6D). EGFP-tagged ADD1^{-ex15} and ADD1^{+ex15} were expressed in cells and then pulled down to detect the phosphorylation level by anti-phospho-(Ser/Thr) antibody. We found that the relative phosphorylation level was significantly decreased in fetal adducin 1 compared to the adult isoform (Figure 6D, E).

Alterations in dendritic spine dynamics in *Mbnl2* KO neurons

Since dendritic spine density in *Mbnl2* KO mice was altered, we further investigated the dendritic spine dynamics by utilising transcranial two-photon imaging, a routine experiment in our lab.³⁴ We performed thinned-skull preparation on *Mbnl2*^{+/+} and *Mbnl2*^{ff} mice

electroporated with pCAG-Cre and pCALNL-GFP (Figure 7A). The initial images were taken on Day 0 (P30) and the same dendrites and spines were re-evaluated on Day 2 (P32) (Figure 7B, C). We found spine elimination rate was significantly higher than the formation rate in *Mbnl2*^{+/+} mice (elimination rate: 32.07 \pm 2.17%; formation rate: 21.76 \pm 2.75%; mice *n* = 4, dendrites *n* = 17) (Figure 7C, D), compatible with the pruning process. On the other hand, *Mbnl2* KO neurons showed nearly equivalent elimination and formation rate (elimination rate: 22.32 \pm 1.99%; formation rate: 22.11 \pm 2.74%; mice *n* = 7, dendrites *n* = 24) as well as a higher rate of stable spines, compared to WT neurons (*Mbnl2*^{+/+} stable rate: 64.74 \pm 2.14%, mice *n* = 4, dendrites *n* = 17; *Mbnl2*^{ff} stable rate: 77.68 \pm 1.99%, mice *n* = 7, dendrites *n* = 24) (Figure 7C, D). These results suggest that *Mbnl2* ablation in neurons may negatively impact the normal pruning process of dendritic spines during adolescence.

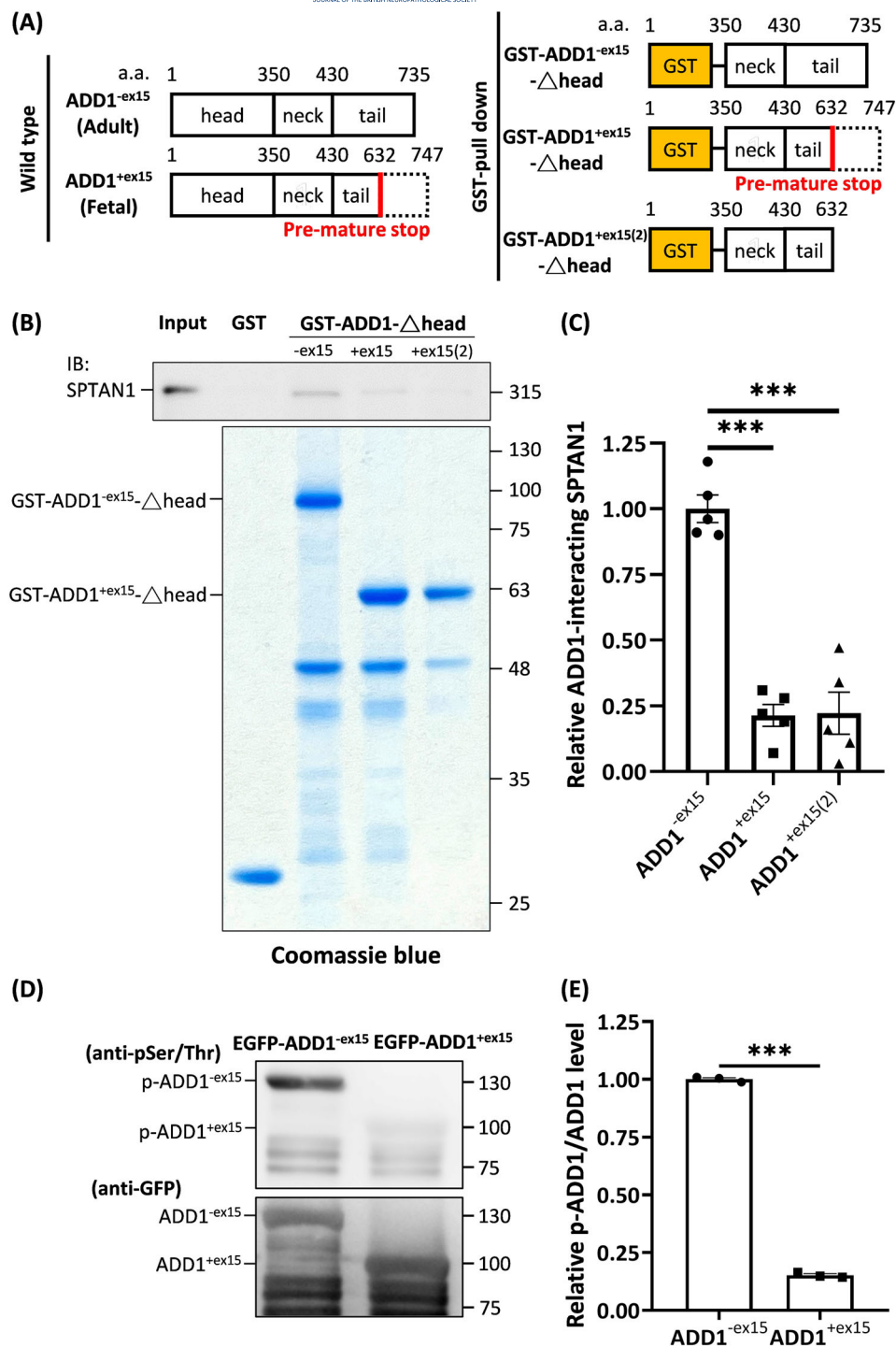


FIGURE 6 SPTAN1 binding and phosphorylation of adult and fetal ADD1 isoforms. (A) Head (1–350 a.a.), neck (351–430 a.a.) and tail (adult: 431–735 a.a.; fetal: 431–747 a.a.) domains of adducin 1 adult and fetal isoforms. The head domain was replaced with GST-tag in all ADD1 constructs for GST pull-down assay. For the fetal isoform, two GST-tagged constructs (350–747 a.a. with a pre-mature STOP codon in one and 350–632 a.a. in another) were generated. (B) GST pull-down assay to determine the interaction between ADD1 and SPTAN1. Brain lysates were incubated with glutathione-agarose beads preloaded with GST, GST-tagged ADD1^{-ex15}-Δhead, GST-tagged ADD1^{+ex15}-Δhead and GST-tagged ADD1^{+ex15(2)}-Δhead and stained with Coomassie blue (lower panel). We used 2% of the input as the positive control. Western blot showed that SPTAN1 (upper panel) was pulled down by ADD1^{-ex15}-Δhead but not ADD1^{+ex15}-Δhead and ADD1^{+ex15(2)}-Δhead. (C) Bar and dot graphs show the relative SPTAN1 interaction between each ADD1 isoform. $n = 5$ mice in each group. Error bars represent SEM. One-way ANOVA test. *** $p < 0.001$. (D) Phosphorylation of ADD1 in HEK293T cells transfected with pEGFP-Add1^{-ex15} and pEGFP-Add1^{+ex15}. ADD1 was pulled down by GFP-trap magnetic beads and blotted by anti-Ser/Thr and anti-GFP antibodies. (E) Bar and dot graphs show a decrease in the phosphorylation of fetal ADD1^{+ex15} isoform. Error bars represent SEM. Student's t-test with Welch's correction. *** $p < 0.001$.

DISCUSSION

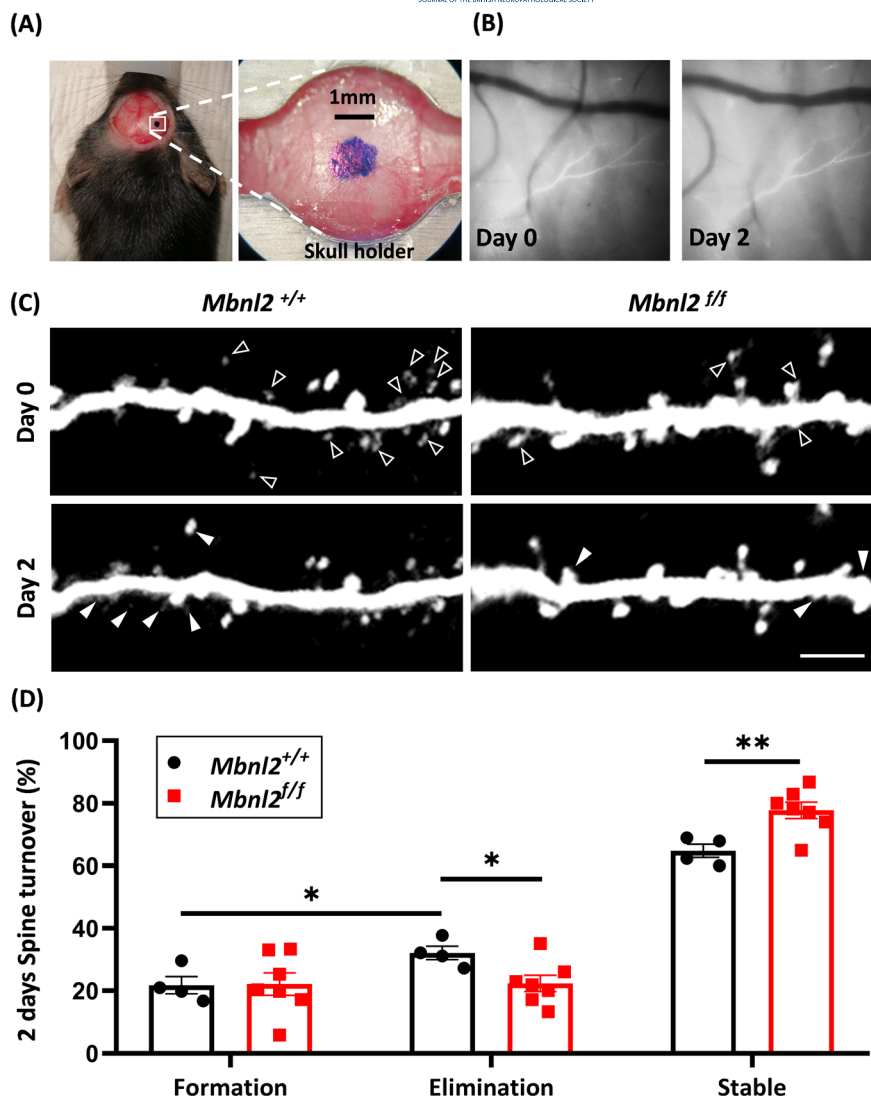
Dendritic spines are post-synaptic structures critical for synaptic plasticity. They receive excitatory inputs and undergo morphological changes in response to environmental cues and accumulated experiences throughout life.^{43,51} These dynamic modulations of dendritic spines play key roles in high cognitive functions including the formation of memory. During the early stage of brain development, the number of synapses increases strikingly from neonatal to young

adulthood.^{51–53} Since the expression of MBNL1/2 proteins also surges postnatally, and mouse model studies demonstrated DM adult brain phenotypes,^{16,26,27} we hypothesized the identified CNS syndrome is caused by alterations of spinogenesis during early development and highly suspected the ablation of MBNL2 in neurons may alter the microstructure and dynamics of dendritic spines (Figure 8).

In the current study, we performed IUE at E14.5 to introduce Cre-recombinase along with GFP into *Mbnl2*-floxed mice to specifically delete *Mbnl2* in neural progenitors in situ. Electroporated GFP⁺

FIGURE 7 Alterations of dendritic spine dynamics in *Mbnl2* KO cortical neurons.

(A) Thinned skull preparation for the observation of spine dynamics using in vivo two-photon microscopy. The mouse head was fixed on a metal holder and a small area of the skull was gently scraped. Bar = 1 mm. (B) Images taken under visible light at experimental day 0 (P30) and day 2 (P32). Blood vessels in the brain were used for positioning neurons. (C) Dynamics of representative dendritic spines from cortical neurons electroporated with Cre-recombinase in *Mbnl2*^{+/+} and *Mbnl2*^{f/f} mice. Emerged new spines (solid arrowheads) and disappeared old spines (hollow arrowheads) were marked accordingly. (D) Bar and dot graphs showing the ratio of spine formation, elimination, and stability ($n = 7$ mice; 24 dendrites) compared to *Mbnl2*^{+/+} mice ($n = 4$ mice; 17 dendrites). Error bars represent SEM, Student's *t*-test. * $p < 0.05$, ** $p < 0.01$.



cells are mostly fated to become cortical layer II/III neurons. Since moderate neuronal migration defects were found previously in *Nestin-Cre* double knockouts (*Mbnl1*^{ΔE3/ΔE3}; *Mbnl2*^{f/f}; *Nestin-Cre*^{+/-}) and *Nestin-Cre* CKOs,²⁶ we first examined several neural developmental processes and found neural progenitors successfully differentiated into NeuN-positive neurons and migrated specifically towards cortical layer II/III. The differences in timing and targeted cell types of knockout may contribute to the discrepancy between the results of *Nestin-Cre* CKO and IUE-mediated *Mbnl2* KO. Also, the double elimination of MBNL1 and MBNL2 abolished the compensatory effects between the two and may have shown a more distinct phenotype on migration.

Here, we studied the somatosensory area of the cortex. Clinically, structural changes of the somatosensory cortex have also been reported in DM patients.^{54,55} In a study of DM2 patients, atrophy was found in the white matter of the cingulate gyrus, medial frontal cortex and primary somatosensory cortex.⁵⁴ A more recent study also reported that the number of CTG repeats in the leukocytes of DM1 patients was significantly correlated to the thickness of the left primary somatosensory cortex.⁵⁵ These findings based on structural

magnetic resonance imaging implicated that the function of the somatosensory cortex may also be affected in DM patients. In our study, we reported the reduction of dendritic spine density and dynamics in the somatosensory cortex in the DM mouse model. These results may provide insights into the cellular basis for the pathogenesis of these areas in DM brains.

Although our study focused on pyramidal neurons in the cortex, changes in inhibitory interneurons may also contribute to brain dysfunction in DM patients. Some DM patients display epileptic assaults^{56–58} and mild cortical changes in the density and distribution of inhibitory interneurons were found in the *Mbnl2*^{f/f}; *Nestin-Cre*^{+/-} mice.²⁶ Abnormality in the small group of inhibitory interneurons may result in improper synaptic transmission in the brain. In addition, although our IUE-mediated *Mbnl2* KO mice did not show obvious changes in morphologies and densities of glial cells in the cortex, glial cells may also play important roles in modulating multiple neuronal functions, including neurotransmitter metabolism, synaptic structure, and blood-brain barrier integrity.⁵⁹ Recently, mis-splicing of genes in primary astrocytes derived from the DMSXL mouse model of DM was

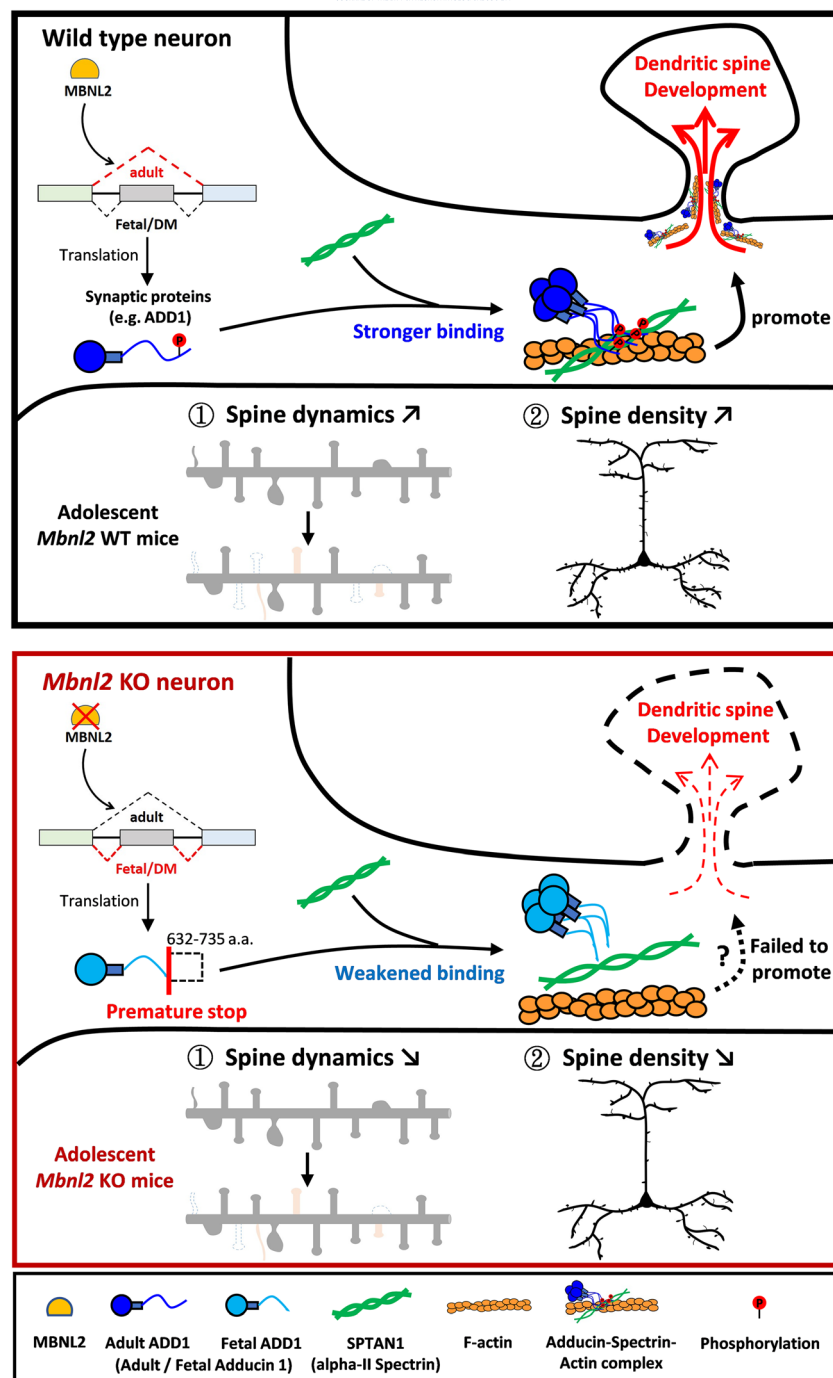


FIGURE 8 Schematic model of MBNL2 in the regulation of spinogenesis. In WT cortical neurons, MBNL2 protein modulates alternative splicing for many synaptic proteins after birth and promotes dendritic spine development. Among them, ADD1 plays a crucial role in spine formation through phosphorylation in the tail domain and interaction with F-actin and SPTAN1 (top). In the *Mbnl2* KO cortical neurons, mis-splicing of *Add1* causes a premature stop in transcription and truncated ADD1 protein in translation. The lack of ADD1 C-terminal tail leads to less phosphorylation and prohibits the interaction between ADD1 (adducin 1) and SPTAN1 (alpha-II spectrin). These changes may disturb the formation of the adducin-spectrin-actin complex and further lead to a decrease in spine dynamics and density in the mouse model of DM (bottom).

reported.^{60,61} Some of the physiological functions of astrocytes may be affected due to changes in RNA splicing. Therefore, the cellular roles of interneurons and glial cells in DM deserve further investigation.

The development of dendritic structures is a crucial process for mature neurons after neuronal migration.⁶² Appropriate types and dynamics of dendritic spines are the basics for maintaining neural plasticity and connectivity in the brain. Misregulations of spinogenesis have been associated with mental disorders and neurodegenerative and neurodevelopmental diseases.^{43,63–65} Although this study could

not rule out the possible contribution of *Mbnl2* knockout to spine development during embryonic stages, we observed decreases in spine densities in the *Mbnl2* KO neurons at P21 and P30, suggesting the loss of MBNL2 expression may compromise spinogenesis or enhanced pruning process. The direct effects on spinogenesis in affected young mice between P14 and P21 remain to be investigated by two-photon microscopy on live animals, which is technically much more challenging.

Spine dynamics was determined by spine formation and elimination, the ratio between formation rate and elimination rate will lead to

an increase or decrease in spine density.⁶⁶ We found the percentage of stable spines was significantly higher in *Mbnl2* KO than in WT, and the proportion of eliminated spines was relatively low in *Mbnl2* KO neurons. The changes in spine dynamics suggested that spine plasticity may also be affected around P30 and eventually lead to the unexpected increase of spine density in *Mbnl2* KO mice at P90. A moderate pruning process after spinogenesis has been considered important for fine-tuning neural circuits, memory consolidation of learning and maturation of cognitive function.^{43,66} Deficient or excessive adolescent spine pruning may impair cognitive function and lead to neurodevelopmental and psychiatric disorders.^{43,66} Our finding in abnormal dendritic spine dynamics in adolescent *Mbnl2* knockout mice may implicate that CNS symptoms may result from abnormal spine formation at early developmental stages, as well as improper spine pruning during adolescence.

The number of dendritic branches is one of the key factors associated with brain connectivity and intelligence quotient (IQ) score.⁶⁷ Based on Sholl analysis in the Cre-electroporated neurons in *Mbnl2*^{f/f} mice at 1 and 3 months old, we did not find significant abnormality in dendritic branches. In our previous study, a significant reduction of basal dendritic branches and a relatively minor decrease in apical dendrites were found in the layer II/III cortical neurons in *Mbnl2*^{f/f}; *Nestin-Cre* mice at 2 to 4 months old.²⁶ In another DM mouse model, EpA960/CaMKII-Cre mouse, which expresses 960 CUG repeats, apical dendrites were not affected until 6 months old but present shortened dendrites at 9 months old.⁶⁸ In primary hippocampal neurons transfected with human DMPK 3' UTR with CUG repeats (DMPK-CUG⁹⁶⁰), they showed decreases in dendrite number compared to control neurons.⁶⁹ These results implicated that age, neuronal type and cell non-autonomous effects may contribute to different complexity of dendritic morphology.

Previously, *Mbnl2* knockout mice enhanced fetal exon inclusion of *Add1* at the RNA level.¹⁶ HITS-CLIP was used to detect target RNAs containing direct binding sites for MBNL2 in vivo and identified potential binding sites within the *Add1* gene. Here, we further showed the shift of ADD1 isoforms in the protein level (Figure 4). Mis-splicing and change of reading frame of ADD1 caused a truncated adducin 1 protein, which lacks MARCKS (myristoylated alanine-rich C-kinase substrate) domain in the C-terminal tail. The MARCKS domain is required for the interaction between adducin 1 and spectrin-actin complex, which is critical in dendritic spine formation/maturation and brain development.⁷⁰⁻⁷³ By in vitro pull-down assay, we demonstrated a reduced binding affinity between fetal adducin 1 isoform and alpha-II spectrin, compared to the adult isoform. Lack of tail domain also led to less phosphorylation of ADD1 fetal isoform. We have examined the sequences of TANC2 and DLG2 fetal isoforms and found that the premature stop codon did not eliminate known/predicted phosphorylation sites. However, it is still possible phosphorylation or other post-translation modification could be changed on TANC2 or DLG2. In fact, knockout of *Add2*, which usually forms dimer/tetramer with adducin 1, has been reported to cause decreases in mushroom spine density and learning/coordination deficits in mice.^{50,74,75} Our results are compatible with previous reports and

implicated that *Add1* may be one of the important genes involved in spinogenesis mediated by MBNL2 and may at least in part account for CNS manifestations in DM patients. It was also quite interesting that there was no significant difference in the spine density at P14, whereas the ADD1 isoform shift has already shown a difference. Therefore, other players may contribute to the defects in dendritic spine development in the context of MBNL2 deficiency at this stage. Although ADD1 has been shown to associate with cerebrovascular/cardiovascular diseases and cancers through its roles in red blood cells and cancer cells,⁷⁶ the contribution of these functions in DM pathogenesis in other tissues remains to be determined.

CONCLUSIONS

In conclusion, we used an IUE-mediated *Mbnl2* knockout model to investigate the functional roles of MBNL2 in the developing cerebral cortex. We found that MBNL2 plays a crucial role in dendritic spine formation and dynamics and results in the shift of isoform expression in synaptic protein ADD1. This study provided morphological evidence of alterations in cortical neurons in a DM mouse model and a potential molecular link to brain manifestations in DM patients.

AUTHOR CONTRIBUTIONS

C.W.H., K.Y.L. and J.W.T. conceptualised the project and designed the experiments. C.W.H., P.T.L., F.S.N., H.Y.C., C.H.C., C.Y.L., C.S., C.L. and Y.F.C. conducted cell and animal experiments. C.W.H., K.Y.L., P.T.L., F.S.N., H.Y.C., C.H.C., C.Y.L., Y.L.S., C.S., C.L., Y.F.C., M.H.L. and J.W.T. analysed and interpreted the data. C.W.H., K.Y.L., P.T.L. and J.W.T. wrote the manuscript. All authors read and revised the manuscript.

ACKNOWLEDGEMENTS

This study is supported by funding from the Ministry of Science and Technology, Taiwan (107-2221-E-010-014, 108-2638-B-010-001-MY2, 108-2321-B-010-011-MY2 and 110-2628-B-A49A-506), Taipei Veterans General Hospital-University System of Taiwan (VGHUST110-G1-5-3), National Health Research Institutes, Taiwan (NHRI-EX109-10904NI), the Brain Research Center, National Yang Ming Chiao Tung University (NYCU) through the Featured Areas Research Center Program within the framework of the Higher Education Sprout Project by the Ministry of Education, Taiwan and ASUS-TeK Computer Inc. through the ASUS-NYCU Industry-Academia Collaboration Research Grant (110J041) to JWT and Chang Gung Memorial Hospital, Keelung Branch (CMRPG2F0502), to KYL.

CONFLICT OF INTEREST

None of the authors reports any conflict of interest.

DATA AVAILABILITY STATEMENT

The data that support the findings of this study are available from the corresponding author upon reasonable request.

ETHICS STATEMENT

All animal studies followed the protocol approved by the Institutional Animal Care and Use Committee at Chang Gung Memorial Hospital, Keelung branch (IACUC No.2016060302).

ORCID

Jin-Wu Tsai  <https://orcid.org/0000-0003-0135-759X>

REFERENCES

- Thornton CA. Myotonic dystrophy. *Neurol Clin*. 2014;32(3):705-719, viii. doi:10.1016/j.ncl.2014.04.011
- Weninger S, Montagnese F, Schoser B. Core clinical phenotypes in myotonic dystrophies. *Front Neurol*. 2018;9:303. doi:10.3389/fneur.2018.00303
- Johnson NE, Butterfield RJ, Mayne K, et al. Population-based prevalence of myotonic dystrophy type 1 using genetic analysis of state-wide blood screening program. *Neurology*. 2021;96(7):e1045-e1053. doi:10.1212/WNL.00000000000011425
- Turner C, Hilton-Jones D. Myotonic dystrophy: diagnosis, management and new therapies. *Curr Opin Neurol*. 2014;27(5):599-606. doi:10.1097/WCO.0000000000000128
- Gourdon G, Meola G. Myotonic dystrophies: state of the art of new therapeutic developments for the CNS. *Front Cell Neurosci*. 2017;11:101. doi:10.3389/fncel.2017.00101
- Fu YH, Pizzuti A, Fenwick RG Jr, et al. An unstable triplet repeat in a gene related to myotonic muscular dystrophy. *Science*. 1992;255(5049):1256-1258. doi:10.1126/science.1546326
- Liquori CL, Ricker K, Moseley ML, et al. Myotonic dystrophy type 2 caused by a CCTG expansion in intron 1 of ZNF9. *Science*. 2001;293(5531):864-867. doi:10.1126/science.1062125
- Aslanidis C, Jansen G, Amemiya C, et al. Cloning of the essential myotonic dystrophy region and mapping of the putative defect. *Nature*. 1992;355(6360):548-551. doi:10.1038/355548a0
- Brook JD, McCurrach ME, Harley HG, et al. Molecular basis of myotonic dystrophy: expansion of a trinucleotide (CTG) repeat at the 3' end of a transcript encoding a protein kinase family member. *Cell*. 1992;69(2):385. doi:10.1016/0092-8674(92)90418-c
- Mahadevan M, Tsilfidis C, Sabourin L, et al. Myotonic dystrophy mutation: an unstable CTG repeat in the 3' untranslated region of the gene. *Science*. 1992;255(5049):1253-1255. doi:10.1126/science.1546325
- Ranum LP, Day JW. Myotonic dystrophy: RNA pathogenesis comes into focus. *Am J Hum Genet*. 2004;74(5):793-804. doi:10.1086/383590
- Miller JW, Urbinati CR, Teng-Umuay P, et al. Recruitment of human muscleblind proteins to (CUG)(n) expansions associated with myotonic dystrophy. *EMBO j*. 2000;19(17):4439-4448. doi:10.1093/emboj/19.17.4439
- Kuyumcu-Martinez NM, Wang GS, Cooper TA. Increased steady-state levels of CUGBP1 in myotonic dystrophy 1 are due to PKC-mediated hyperphosphorylation. *Mol Cell*. 2007;28(1):68-78. doi:10.1016/j.molcel.2007.07.027
- Mankodi A, Logigian E, Callahan L, et al. Myotonic dystrophy in transgenic mice expressing an expanded CUG repeat. *Science*. 2000;289(5485):1769-1773. doi:10.1126/science.289.5485.1769
- Mankodi A, Urbinati CR, Yuan QP, et al. Muscleblind localizes to nuclear foci of aberrant RNA in myotonic dystrophy types 1 and 2. *Hum Mol Genet*. 2001;10(19):2165-2170. doi:10.1093/hmg/10.19.2165
- Charizanis K, Lee KY, Batra R, et al. Muscleblind-like 2-mediated alternative splicing in the developing brain and dysregulation in myotonic dystrophy. *Neuron*. 2012;75(3):437-450. doi:10.1016/j.neuron.2012.05.029
- Lee KY, Li M, Manchanda M, et al. Compound loss of muscleblind-like function in myotonic dystrophy. *EMBO Mol Med*. 2013;5(12):1887-1900. doi:10.1002/emmm.201303275
- Kanadia RN, Johnstone KA, Mankodi A, et al. A muscleblind knock-out model for myotonic dystrophy. *Science*. 2003;302(5652):1978-1980. doi:10.1126/science.1088583
- Thomas JD, Sznajder LJ, Bardhi O, et al. Disrupted prenatal RNA processing and myogenesis in congenital myotonic dystrophy. Research Support, Non-U.S. Gov't Research Support, N.I.H., Extramural. *Genes Dev*. 2017;31(11):1122-1133. doi:10.1101/gad.300590.117
- Johnson NE, Luebbe E, Eastwood E, Chin N, Moxley RT 3rd, Heatwole CR. The impact of congenital and childhood myotonic dystrophy on quality of life: a qualitative study of associated symptoms. *J Child Neurol*. 2014;29(7):983-986. doi:10.1177/0883073813484804
- Prasad M, Hicks R, MacKay M, Nguyen CT, Campbell C. Developmental milestones and quality of life assessment in a congenital myotonic dystrophy cohort. *J Neuromuscul Dis*. 2016;3(3):405-412. doi:10.3233/JND-160165
- Minnerop M, Weber B, Schoene-Bake JC, et al. The brain in myotonic dystrophy 1 and 2: evidence for a predominant white matter disease. *Brain*. 2011;134(Pt 12):3530-3546. doi:10.1093/brain/awr299
- Wozniak JR, Mueller BA, Lim KO, Hemmy LS, Day JW. Tractography reveals diffuse white matter abnormalities in myotonic dystrophy type 1. *J Neurol Sci*. 2014;341(1-2):73-78. doi:10.1016/j.jns.2014.04.005
- Zanigni S, Evangelisti S, Giannoccaro MP, et al. Relationship of white and gray matter abnormalities to clinical and genetic features in myotonic dystrophy type 1. *Neuroimage Clin*. 2016;11:678-685. doi:10.1016/j.nicl.2016.04.012
- Minnerop M, Gliem C, Kornblum C. Current Progress in CNS imaging of myotonic dystrophy. *Front Neurol*. 2018;9:646. doi:10.3389/fneur.2018.00646
- Lee KY, Chang HC, Seah C, Lee LJ. Deprivation of Muscleblind-like proteins causes deficits in cortical neuron distribution and morphological changes in dendritic spines and postsynaptic densities. *Front Neuroanat*. 2019;13:75. doi:10.3389/fnana.2019.00075
- Goodwin M, Mohan A, Batra R, et al. MBNL sequestration by toxic RNAs and RNA misprocessing in the myotonic dystrophy brain. *Cell Rep*. 2015;12(7):1159-1168. doi:10.1016/j.celrep.2015.07.029
- Chen YA, Lu IL, Tsai JW. Contactin-1/F3 regulates neuronal migration and morphogenesis through modulating RhoA activity. *Front Mol Neurosci*. 2018;11:422. doi:10.3389/fnmol.2018.00422
- Lu IL, Chen C, Tung CY, et al. Identification of genes associated with cortical malformation using a transposon-mediated somatic mutagenesis screen in mice. *Nat Commun*. 2018;9(1):2498. doi:10.1038/s41467-018-04880-8
- Chen JL, Chang CH, Tsai JW. Gli2 rescues delays in brain development induced by Kif3a dysfunction. *Cereb Cortex*. 2019;29(2):751-764. doi:10.1093/cercor/bhx356
- Tsai MH, Cheng HY, Nian FS, et al. Impairment in dynein-mediated nuclear translocation by BICD2 C-terminal truncation leads to neuronal migration defect and human brain malformation. *Acta Neuropathol Commun*. 2020;8(1):106. doi:10.1186/s40478-020-00971-0
- Tsai MH, Muir AM, Wang WJ, et al. Pathogenic variants in CEP85L cause sporadic and familial posterior predominant Lissencephaly. *Neuron*. 2020;106(2):237-245 e8. doi:10.1016/j.neuron.2020.01.027
- Liu YT, Nian FS, Chou WJ, et al. PRRT2 mutations lead to neuronal dysfunction and neurodevelopmental defects. *Oncotarget*. 2016;7(26):39184-39196. doi:10.18632/oncotarget.9258
- Ma L, Qiao Q, Tsai JW, Yang G, Li W, Gan WB. Experience-dependent plasticity of dendritic spines of layer 2/3 pyramidal neurons in the mouse cortex. *Dev Neurobiol*. 2016;76(3):277-286. doi:10.1002/dneu.22313

35. Jarrard LE. On the role of the hippocampus in learning and memory in the rat. *Behav Neural Biol.* 1993;60(1):9-26. doi:[10.1016/0163-1047\(93\)90664-4](https://doi.org/10.1016/0163-1047(93)90664-4)
36. Kempermann G, Jessberger S, Steiner B, Kronenberg G. Milestones of neuronal development in the adult hippocampus. *Trends Neurosci.* 2004;27(8):447-452. doi:[10.1016/j.tins.2004.05.013](https://doi.org/10.1016/j.tins.2004.05.013)
37. Vadodaria KC, Gage FH. SnapShot: adult hippocampal neurogenesis. *Cell.* 2014;156(5):1114-1114 e1. doi:[10.1016/j.cell.2014.02.029](https://doi.org/10.1016/j.cell.2014.02.029)
38. Brandt MD, Jessberger S, Steiner B, et al. Transient calretinin expression defines early postmitotic step of neuronal differentiation in adult hippocampal neurogenesis of mice. *Mol Cell Neurosci.* 2003;24(3):603-613. doi:[10.1016/s1044-7431\(03\)00207-0](https://doi.org/10.1016/s1044-7431(03)00207-0)
39. Baimbridge KG, Miller JJ. Immunohistochemical localization of calcium-binding protein in the cerebellum, hippocampal formation and olfactory bulb of the rat. *Brain Res.* 1982;245(2):223-229. doi:[10.1016/0006-8993\(82\)90804-6](https://doi.org/10.1016/0006-8993(82)90804-6)
40. Matsuda T, Cepko CL. Controlled expression of transgenes introduced by in vivo electroporation. *Proc Natl Acad Sci U S A.* 2007;104(3):1027-1032. doi:[10.1073/pnas.0610155104](https://doi.org/10.1073/pnas.0610155104)
41. Sugitani Y, Nakai S, Minowa O, et al. Brn-1 and Brn-2 share crucial roles in the production and positioning of mouse neocortical neurons. *Genes Dev.* 2002;16(14):1760-1765. doi:[10.1101/gad.978002](https://doi.org/10.1101/gad.978002)
42. Mullen RJ, Buck CR, Smith AM. NeuN, a neuronal specific nuclear protein in vertebrates. *Development.* 1992;116(1):201-211. doi:[10.1242/dev.116.1.201](https://doi.org/10.1242/dev.116.1.201)
43. Runge K, Cardoso C, de Chevigny A. Dendritic spine plasticity: function and mechanisms. *Front Synaptic Neurosci.* 2020;12:36. doi:[10.3389/fnsyn.2020.00036](https://doi.org/10.3389/fnsyn.2020.00036)
44. Berry KP, Nedivi E. Spine dynamics: are they all the same? *Neuron.* 2017;96(1):43-55. doi:[10.1016/j.neuron.2017.08.008](https://doi.org/10.1016/j.neuron.2017.08.008)
45. Sun Q, Turrigiano GG. PSD-95 and PSD-93 play critical but distinct roles in synaptic scaling up and down. *J Neurosci.* 2011;31(18):6800-6808. doi:[10.1523/JNEUROSCI.5616-10.2011](https://doi.org/10.1523/JNEUROSCI.5616-10.2011)
46. Favaro PD, Huang X, Hosang L, et al. An opposing function of paralogs in balancing developmental synapse maturation. *PLoS Biol.* 2018;16(12):e2006838. doi:[10.1371/journal.pbio.2006838](https://doi.org/10.1371/journal.pbio.2006838)
47. Han S, Nam J, Li Y, et al. Regulation of dendritic spines, spatial memory, and embryonic development by the TANC family of PSD-95-interacting proteins. *J Neurosci.* 2010;30(45):15102-15112. doi:[10.1523/JNEUROSCI.3128-10.2010](https://doi.org/10.1523/JNEUROSCI.3128-10.2010)
48. Matsuoka Y, Li X, Bennett V. Adducin is an in vivo substrate for protein kinase C: phosphorylation in the MARCKS-related domain inhibits activity in promoting spectrin-actin complexes and occurs in many cells, including dendritic spines of neurons. *J Cell Biol.* 1998;142(2):485-497. doi:[10.1083/jcb.142.2.485](https://doi.org/10.1083/jcb.142.2.485)
49. Li X, Matsuoka Y, Bennett V. Adducin preferentially recruits spectrin to the fast growing ends of actin filaments in a complex requiring the MARCKS-related domain and a newly defined oligomerization domain. *J Biol Chem.* 1998;273(30):19329-19338. doi:[10.1074/jbc.273.30.19329](https://doi.org/10.1074/jbc.273.30.19329)
50. Bednarek E, Caroni P. Beta-adducin is required for stable assembly of new synapses and improved memory upon environmental enrichment. *Neuron.* 2011;69(6):1132-1146. doi:[10.1016/j.neuron.2011.02.034](https://doi.org/10.1016/j.neuron.2011.02.034)
51. Markus EJ, Petit TL. Neocortical synaptogenesis, aging, and behavior: lifespan development in the motor-sensory system of the rat. *Exp Neurol.* 1987;96(2):262-278. doi:[10.1016/0014-4886\(87\)90045-8](https://doi.org/10.1016/0014-4886(87)90045-8)
52. Rakic P, Bourgeois JP, Eckenhoff MF, Zecevic N, Goldman-Rakic PS. Concurrent overproduction of synapses in diverse regions of the primate cerebral cortex. *Science.* 1986;232(4747):232-235. doi:[10.1126/science.3952506](https://doi.org/10.1126/science.3952506)
53. Huttenlocher PR. Morphometric study of human cerebral cortex development. *Neuropsychologia.* 1990;28(6):517-527. doi:[10.1016/0028-3932\(90\)90031-i](https://doi.org/10.1016/0028-3932(90)90031-i)
54. Schneider-Gold C, Bellenberg B, Prehn C, et al. Cortical and subcortical grey and white matter atrophy in myotonic dystrophies type 1 and 2 is associated with cognitive impairment, depression and daytime sleepiness. *PLoS ONE.* 2015;10(6):e0130352. doi:[10.1371/journal.pone.0130352](https://doi.org/10.1371/journal.pone.0130352)
55. Serra L, Bianchi G, Bruschini M, et al. Abnormal cortical thickness is associated with deficits in social cognition in patients with myotonic dystrophy type 1. *Front Neurol.* 2020;11:113. doi:[10.3389/fneur.2020.00113](https://doi.org/10.3389/fneur.2020.00113)
56. Meola G, Sansone V. Cerebral involvement in myotonic dystrophies. *Muscle Nerve.* 2007;36(3):294-306. doi:[10.1002/mus.20800](https://doi.org/10.1002/mus.20800)
57. Worku DK. Concurrence of myotonic dystrophy and epilepsy: a case report. *J Med Case Reports.* 2014;8(1):427. doi:[10.1186/1752-1947-8-427](https://doi.org/10.1186/1752-1947-8-427)
58. Peddareddygar LR, Grewal AS, Grewal RP. Focal seizures in a patient with myotonic disorder type 2 co-segregating with a chloride voltage-gated channel 1 gene mutation: a case report. *J Med Case Reports.* 2016;10:167. doi:[10.1186/s13256-016-0958-8](https://doi.org/10.1186/s13256-016-0958-8)
59. Patel DC, Tewari BP, Chaunsali L, Sontheimer H. Neuron-glia interactions in the pathophysiology of epilepsy. *Nat Rev Neurosci.* 2019;20(5):282-297. doi:[10.1038/s41583-019-0126-4](https://doi.org/10.1038/s41583-019-0126-4)
60. Gonzalez-Barriga A, Lallemand L, Dinca DM, et al. Integrative cell type-specific multi-omics approaches reveal impaired programs of glial cell differentiation in mouse culture models of DM1. *Front Cell Neurosci.* 2021;15:662035. doi:[10.3389/fncel.2021.662035](https://doi.org/10.3389/fncel.2021.662035)
61. Dinca DM, Lallemand L, Gonzalez-Barriga A, et al. Myotonic dystrophy RNA toxicity alters morphology, adhesion and migration of mouse and human astrocytes. *Nat Commun.* 2022;13(1):3841. doi:[10.1038/s41467-022-31594-9](https://doi.org/10.1038/s41467-022-31594-9)
62. Meltzer S, Chen C. Balancing dendrite morphogenesis and neuronal migration during cortical development. *J Neurosci.* 2016;36(42):10726-10728. doi:[10.1523/JNEUROSCI.2425-16.2016](https://doi.org/10.1523/JNEUROSCI.2425-16.2016)
63. Penzes P, Cahill ME, Jones KA, VanLeeuwen JE, Woolfrey KM. Dendritic spine pathology in neuropsychiatric disorders. *Nat Neurosci.* 2011;14(3):285-293. doi:[10.1038/nn.2741](https://doi.org/10.1038/nn.2741)
64. Phillips M, Pozzo-Miller L. Dendritic spine dysgenesis in autism related disorders. *Neurosci Lett.* 2015;601:30-40. doi:[10.1016/j.neulet.2015.01.011](https://doi.org/10.1016/j.neulet.2015.01.011)
65. Herms J, Dorostkar MM. Dendritic spine pathology in neurodegenerative diseases. *Annu Rev Pathol.* 2016;11(1):221-250. doi:[10.1146/annurev-pathol-012615-044216](https://doi.org/10.1146/annurev-pathol-012615-044216)
66. Stein IS, Zito K. Dendritic spine elimination: molecular mechanisms and implications. *Neuroscientist.* 2019;25(1):27-47. doi:[10.1177/1073858418769644](https://doi.org/10.1177/1073858418769644)
67. Quach TT, Stratton HJ, Khanna R, et al. Intellectual disability: dendritic anomalies and emerging genetic perspectives. *Acta Neuropathol.* 2021;141(2):139-158. doi:[10.1007/s00401-020-02244-5](https://doi.org/10.1007/s00401-020-02244-5)
68. Wang PY, Lin YM, Wang LH, Kuo TY, Cheng SJ, Wang GS. Reduced cytoplasmic MBNL1 is an early event in a brain-specific mouse model of myotonic dystrophy. *Hum Mol Genet.* 2017;26(12):2247-2257. doi:[10.1093/hmg/ddx115](https://doi.org/10.1093/hmg/ddx115)
69. Wang PY, Chang KT, Lin YM, Kuo TY, Wang GS. Ubiquitination of MBNL1 is required for its cytoplasmic localization and function in promoting neurite outgrowth. *Cell Rep.* 2018;22(9):2294-2306. doi:[10.1016/j.celrep.2018.02.025](https://doi.org/10.1016/j.celrep.2018.02.025)
70. Nestor MW, Cai X, Stone MR, Bloch RJ, Thompson SM. The actin binding domain of beta-spectrin regulates the morphological and functional dynamics of dendritic spines. *PLoS ONE.* 2011;6(1):e16197. doi:[10.1371/journal.pone.0016197](https://doi.org/10.1371/journal.pone.0016197)
71. Efimova N, Korobova F, Stankewich MC, et al. BetaIII spectrin is necessary for formation of the constricted neck of dendritic spines and regulation of synaptic activity in neurons. *J Neurosci.* 2017;37(27):6442-6459. doi:[10.1523/JNEUROSCI.3520-16.2017](https://doi.org/10.1523/JNEUROSCI.3520-16.2017)
72. Han B, Zhou R, Xia C, Zhuang X. Structural organization of the actin-spectrin-based membrane skeleton in dendrites and soma of

- neurons. *Proc Natl Acad Sci U S A*. 2017;114(32):E6678-E6685. doi:[10.1073/pnas.1705043114](https://doi.org/10.1073/pnas.1705043114)
73. Wang Y, Ji T, Nelson AD, et al. Critical roles of alphaspectrin in brain development and epileptic encephalopathy. *J Clin Invest*. 2018; 128(2):760-773. doi:[10.1172/JCI95743](https://doi.org/10.1172/JCI95743)
 74. Porro F, Rosato-Siri M, Leone E, et al. Beta-adducin (Add2) KO mice show synaptic plasticity, motor coordination and behavioral deficits accompanied by changes in the expression and phosphorylation levels of the alpha- and gamma-adducin subunits. *Genes Brain Behav*. 2010;9(1):84-96. doi:[10.1111/j.1601-183X.2009.00537.x](https://doi.org/10.1111/j.1601-183X.2009.00537.x)
 75. Jung Y, Mulholland PJ, Wiseman SL, Chandler LJ, Picciotto MR. Constitutive knockout of the membrane cytoskeleton protein beta adducin decreases mushroom spine density in the nucleus accumbens but does not prevent spine remodeling in response to cocaine. *Eur J Neurosci*. 2013;37(1):1-9. doi:[10.1111/ejn.12037](https://doi.org/10.1111/ejn.12037)
 76. Kiang KM, Leung GK. A review on adducin from functional to pathological mechanisms: future direction in cancer. *Biomed Res Int*. 2018; 2018:3465929. doi:[10.1155/2018/3465929](https://doi.org/10.1155/2018/3465929)

SUPPORTING INFORMATION

Additional supporting information can be found online in the Supporting Information section at the end of this article.

How to cite this article: Huang C-W, Lee K-Y, Lin P-T, et al. Muscleblind-like 2 knockout shifts adducin 1 isoform expression and alters dendritic spine dynamics of cortical neurons during brain development. *Neuropathol Appl Neurobiol*. 2023;49(2):e12890. doi:[10.1111/nan.12890](https://doi.org/10.1111/nan.12890)